IRSTI 31.15.15:31.15.25:31.21.25:31.27.22:34.27.19:34.47.15 https://doi.org/10.26577/IJBCh20251828

A.V. Sharov[1*], P.A. Nikolaychuk[1, 2], A.A. Tereshkina[1, 3], A.V. Dostovalova[1], Y.A. Enova[1], D.S. Popova[1], D.A. Rychkova[1], A.Y. Kurochkina[1], V.V. Savinova[1], A.N. Nakoskin[1], I.V. Shipitsyna[4], O.V. Filisteev[1], S.T. Lwin[5], M.M. Zaw[5], Z. Minthein[6], Z.Y.M. Oo[1, 7]

[1]Kurgan State University, Kurgan, Russia
[2]Scientific-Educational Centre of Chemistry and Chemical Technology of Novosibirsk State University, Novosibirsk, Russia
[3]Ural Federal University named after the first President of Russia B.N. Yeltsin, Yekaterinburg, Russia
[4]National Ilizarov Medical Research Centre for Traumatology and Orthopedics, Kurgan, Russia
[5]Medical Research Centre, Nay Pyi Taw, Myanmar
[6]Medical Academy, Yangon, Myanmar
[7]Science Research Centre of the Republic of the Union of Myanmar, Nay Pyi Taw, Myanmar
*e-mail: sharow84@gmail.com
*(Received 28 May 2025; received in revised form 19 December 2025; accepted 26 December 2025)*

# A Schiff base 4-chloro-2-((pyridin-3-ylimino)methyl)phenol: crystal structure details, computational study, proteolytic properties, molecular docking, *in vivo* toxicity and *in vitro* antibacterial activity

**Abstract.** IIn the present study, a synthesis, computational modeling and experimental investigation of 4-chloro-2-((pyridin-3-ylimino)methyl)phenol was reported. A Hirshfeld surface analysis was used for elucidation of interatomic contacts to the crystal structure of the substance. A DFT analysis was used for geometry optimisation, modeling of both vibrational and absorption spectra of three tautomeric forms and their comparison with the experimental spectra. The compound exists in the enolimine form in organic solvents, and the addition of water leads to the appearance of the ketoenamine form. A molecular docking was used for estimation of binding of three tautomeric forms with some proteins of *Staphylococcus* aureus and *Pseudomonas aeruginosa*. The ionisation constants in hydroethanolic mixtures are equal to 4.16, 8.55 and 10.43. The results of the antimicrobial tests of microamounts of 4-chloro-2-((pyridin-3-ylimino)methyl)phenol deposited onto the surface of titanium alloy of medical grade against the same microbials, and of the toxicity test of this compound with laboratory mice were provided. An inhibitory activity against *Pseudomonas aeruginosa* was revealed. No significant toxicity e fects of the compound on the laboratory mice was detected.
**Keywords:** Schiff base, crystal structure, Hirshfeld surface analysis, computational study, DFT, molecular docking, toxicity, antibacterial activity.

## Introduction

The secondary imines or the Schiff bases [1], namely the condensation products of aldehydes and amines, are of extensive interest to the researchers for more than 100 years due to a very simple one-pot synthesis procedure and a wide range of potentially practically applicable properties [1–5]. Particularly, several imines have demonstrated antimicrobial properties against common pathogens [6–28], the details are presented in Table S1. Among their diversity, Schiff bases based on salicylic aldehyde, similar compounds, and their derivatives could be pointed out separately. They are characterised by the presence of an intramolecular hydrogen bond and the ability to form various tautomeric enolimine and ketoenamine forms [29–36]. The equilibria of formation of these forms are usually shifted under the influence of external factors, in particular, solvents with different polarity. A variety of their interesting properties of practical significance include optical properties, the complexation ability, the ability to bind nucleic acids, and a wide range of biological properties [10, 19, 27, 37–44].

An attention was recently drawn to the derivatives of salicylic aldehyde with a heterocycle in the amine residue, including from the point of view of their possible application in medicinal chemistry.

This is due, among other things, to the wide use of heterocyclic compounds in medicine [45,46]. First of all, the condensation products of salicylic aldehyde and *ortho*-, *meta*-, and *para*-aminopyridines is of interest. The literature contains several information on the structure, optical properties, complex formation, and biological activity of 2-aminopyridine and 4-aminopyride derivatives [47–56]. However, such staring attention was not yet paid to 3-aminopyridine derivatives, despite their potentially interesting properties. For example, unlike 2- and 4-aminopyridine, 3-aminopyridine has fairly strong basic properties in aqueous solutions due to the redistribution of electron density between the amine nitrogen in the *meta*-position and the heterocyclic nitrogen [57]. This can affect the equilibria of keto-enol tautomerism of Schiff bases and, as a consequence, the properties of the substance in various environments.

In the present study the results of detailisation of the crystal structure using computer algorithms, DFT analysis of the structure and main characteristics of the molecule, determination of some physicochemical properties, molecular docking and *in vitro* analysis of the antimicrobial activity of 4-chloro-2-((pyridin-3-ylimino)methyl)phenol, a compound based on 5-chlorosalicylic aldehyde and 3-aminopyridine, are presented.

Because derivatives of salicylaldehide already demonstrated antimicrobial properties [10, 19], it was also important to test the antimicrobial properties of the synthesised compound. However, instead of using organic solvents for testing, the model samples of the surface of orthopedic implants from medical titanium covered by electrodeposited calcium phosphate material and Schiff base were prepared.

*In vitro* studies were conducted on cultures of both *Staphylococcus aureus* and *Pseudomonas aeruginosa*, namely, the common pathogens that cause infections complicating the osteogenesis processes after surgery. The toxicity of 4-chloro-2-((pyridin-3-ylimino)methyl)phenol was also tested *in vivo* using laboratory mice.Introduction should consist of justification of importance of the field, theoretical and practical significance of the topic, the meaning of the narrow problem, solution for the problem or formulation of hypothesis, the objectives of the work.

## Materials and methods

*Reagents and equipment*

5-chlorosalicylaldehyde (Shanghai Macklin Biochemical Technology Co. Ltd, China), 3-aminopyridine (Sisco Research Laboratories Pvt Ltd., India), calcium nitrate (Reakhim LLC, Russia), ammonium dihydrophosphate (Reakhim LLC, Russia), potassium chloride (Reakhim LLC, Russia), nitric acid (Èkos-1 LLC, Russia), sulphuric acid (Èkos-1 LLC, Russia), ammonium hydroxide (Èkos-1 LLC, Russia), potassium hydroxide (Reakhim LLC, Russia), barium chloride (Reakhim LLC, Russia), barium hydroxide (Reaktiv-Express LLC, Russia), spectral grade potassium bromide (Sigma-Aldrich, USA), standard buffer solutions for pH calibration (Reakhim LLC, Russia), Muller-Hinton agar (Agat-Med LLC, Russia), xylazine, tiletamine, zolazepam and chlorhexidine (obtained from local pharmacies, Russia), and assay kits for determination of liver enzymes (Vital LLC, Russia) were used without further purification. Methanol (Èkos-1 LLC, Russia), ethanol (Èkos-1 LLC, Russia), propan-1-ol (Èkos-1 LLC, Russia), propan-2-ol (Èkos-1 LLC, Russia), butan-1-ol (Èkos-1 LLC, Russia), butan-2-ol (Èkos-1 LLC, Russia), acetone (Èkos-1 LLC, Russia), acetonitrile (Èkos-1 LLC, Russia), chloroform (Èkos-1 LLC, Russia), hexane (Èkos-1 LLC, Russia), toluene (Èkos-1 LLC, Russia) were redistilled before use.

The distilled water was produced using the aquadistiller Puridest PD 4D (Lauda Scientific GmbH, Germany). The samples were weighted using the analytical balance Vibra HT-224RCE (Schinko Denshi Co. Ltd., Japan). Infrared spectra were recorded using the spectrophotometer FT-801 (Simeks LLC, Russia) in KBr pellets. 1H NMR spectra were registered using the spectrometer Bruker DRX-400 (Bruker Corporation, Germany). Absorption spectra were recorded using the spectrophotometer XPOMATPOH XT-500D (LabTex LLC, Russia). The ionometer Mettler-Toledo SevenCompact (Mettler Toledo Corp., Switzerland) equipped with the pH Sensor InLab Expert Pro-ISM (Mettler Toledo Corp., Switzerland) was used for pH measurement and potentiometric titrations. The dry-air thermostat TS-1/20 SPU (JSC «Smolenskoe special'noe konstruktorsko-tehnologičeskoe bûro sistem programmnogo upravleniâ», Russia) was used for sample incubation in microbial tests. The abacterial air medium box BAVnp-01-«Laminar-C»-1,2 Lorica (CJSC «Laminarnye sistemy», Russia) was used for working with bacterial cultures.

Laboratory mice of CBA strain were kindly provided by pharmaceutical company LLC Binnopharm Group, Russia as the gift.

*Synthesis of the compound*

A Schiff base (4-chloro-2-((pyridin-3-ylimino) methyl)phenol, compound **I**, see Figure 1) was obtained in an ethanolic medium using a condensation

reaction of 5-chlorosalicylaldehyde and 3-aminopyridine. To the solution of 5-chlorosalicylaldehyde (1.0292 g, 6.57 mmol) in 10 ml of ethanol, a solution of 3-aminopyridine (0.6188 g, 6.57 mmol) in 10 ml of ethanol were gradually added. The reaction mixture was boiled with the reflux condenser during 4 hours, then cooled to the room temperature. The formed orange precipitate was filtered, washed several times with cold ethanol and dried in vacuum. The yield was 1.4663 g (96 %).

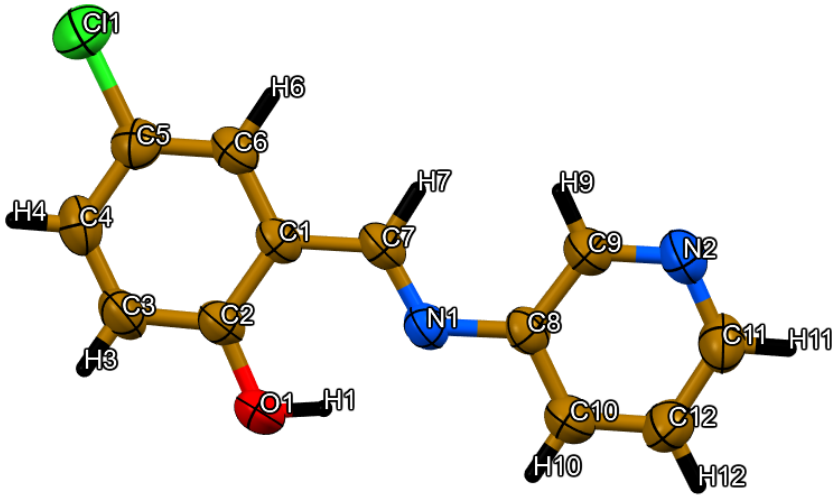


**Figure 1 –** Molecular structure of compound **I** obtained in [47] by X-Ray crystallography

*Compound characterisation*

$^1$H NMR spectra were registered at the frequency of $^1$H equal to 400 MHz in $CDCl_3$. The chemical shifts are depicted relatively to trimethylsilane. IR spectra were registered with the spectral resolution of 4.1 $cm^{-1}$ and the scan number equal to 32 in the potassium bromide pellets. UV-spectra of the compound **I** solutions in the different solvents as well as in hydroethanolic mixtures were registered in quartz cuvettes with the optical path length equal to 1 cm. The scan range was from 190 to 800 nm with the step of 1 nm.

The ionisation constants of **I** were determined with hydroethanolic mixtures with the ethanol mass fraction of 73% by potentiometric titration with the combined pH sensor. The electrode was calibrated using the standard buffer solutions. The corrected pH values in the hydroethanolic mixtures were calculated from the electrode readings using the method proposed by Bates [58], where the medium effect was determined from the experimental data [58, 59]. The measurements were made at the temperature of 298 K and the ionic strength of 0.01 M, maintained by the potassium chloride. The titration of the compound **I** solution was carried out by either hydrochloric acid or potassium hydroxide. Potassium hydroxide was pre-purified from the presence of carbonates by barium hydroxide.

*Hirshfeld surface analysis*

The Hirshfeld surfaces [60–62] of **I** were generated using the Crystal Explorer 17 software [62]. The original crystal structure was taken from the CCDC database with deposition number 1869718 [63, 64]. The 2D fingerprint plots were generated with the Crystal Explorer 17 software and used for description of the intermolecular interactions, including contacts between the pairs of atoms.

*Quantum chemical calculations*

The geometry of the ground state (in gas phase), electronic (in alcoholic solution) и vibrational (in gas phase) spectra were calculated by the density functional theory (DFT) using GaussView 6.0 molecular visualisation program and Gaussian 09 [65, 66], Revision D.01 program package. The functional Becke-3-parametr-Lee-Yang-Parr (B3LYP) and the basis set 6-311++G(d,p) [67 – 69] were employed. The correspondence of the calculated bands in the IR spectra to vibrations of specific atoms or groups of atoms was established using VEDA software [70]. The HOMO and LUMO orbitals and MEP surfaces were generated based on the optimised geometry for the ground state of substance **I** in the gas phase.

*Molecular docking*

The molecular docking procedure was implemented for some proteins (mainly of the cell walls) of *Staphylococcus aureus* and *Pseudomonas aeruginosa*.

Crystal structures of proteins for the molecular docking procedure were taken from the RCSB Protein Data Bank [71]. Processing of molecular models, as well as visualisation of the results of interactions between **I** and active centers of proteins, were performed in BIOVIA Discovery Studio 2020 and AutoDock tools software. Molecular docking was performed with the AutoDock Vina software [72, 73].

*Preparation of the samples containing microamounts of Schiff base for in vitro anti-microbial testing*

The samples have a form of the disks with a diameter of 5 mm and a height of 1 mm made of medical grade titanium alloy Ti-6Al-4V covered by a calcium phosphate coating with additives of **I**. The metal disks were pre-cleaned in an ultrasonic bath and degreased using acetone. Before the precipitation of calcium phosphate, anodic oxidation of titanium was carried out in a 0.5 M $H_2SO_4$ solution [74, 75]. The samples serve as anodes, and a copper cathode was used. Anodisation was carried out at a direct current voltage of 25 V for 1 minute at room temperature. After oxidation, the samples were washed in an ultrasonic bath with distilled water and dried using the filter paper.

The electrolyte for the precipitation of phosphates contained 0.042 M $Ca(NO_3)_2$ and 0.025 M $NH_4H_2PO_4$ [74]. The pH value of the electrolyte was adjusted to 4.1 using nitric acid or ammonium hydroxide solutions. Electrolysis was carried out for 2 hours at a direct current voltage of 4 V. A titanium sample served as a cathode, and graphite rod as an anode. After electrolysis, the samples were washed in distilled water and dried in air. At the last stage, the samples were impregnated with 1 mM ethanol solution of **I** and dried afterwards. The content of the Schiff base in the samples was determined by its extraction from the samples with ethanol, followed by spectrophotometric analysis.

*Spectrophotometric determination of (4-chloro-2-((pyridin-3-ylimino)methyl)phenol*

The concentration of the compound **I** in the ethanolic extracts were determined spectrophotometrically. For this, ten disks (described in the previous section) covered by calcium phosphate and impregnated with compound **I** were immersed into 5 ml of ethanol, vigorously shaken, immersed into another 5 ml of ethanol and vigorously shaken again. The resulting ethanolic solutions were combined, and the content of compound **I** was measured spectrophotometrically at the wavelength of 355 nm with the molar extinction coefficient equal to 1900 $m^2$/mol. The analytical performance of the method is as follows: linearity range equals 0.1 – 20 mg/L, with LOD 0.015 mg/L, and LOQ 0.05 mg/L, recovery studies revealed the relative uncertainty of 3.5% for the 1 mg/L solution, and reproducibility studies revealed the relative standard deviation of 3.2% ($f$ = 5, p = 0.95) for the 1 mg/L solution of compound **I**.

*In vitro antimicrobial tests*

The museum strains *Staphylococcus aureus* ATCC 25923, *Pseudomonas aeruginosa* ATCC 27853, Escherichia coli ATCC 25922 were used as test cultures. A suspension (corresponding to the 0.5 McFarland standard [76]) of the studied microorganism was seeded on a Petri dish with a dense nutrient medium (Muller-Hinton agar, Agat-Med LLC, Russia). The disks described previously were applied to the surface of the agar with microbial cultures. The cultures were incubated in a dry-air thermostat TS-1/20 SPU (JSC «Smolenskoe special'noe konstruktorsko-tehnologičeskoe bûro sistem programmnogo upravleniâ», Russia) for 24 hours at a temperature of 35±1˚C. The results were recorded based on the absence or presence of microorganism growth around the disk, measuring the diameter of the growth inhibition zone.

*In vivo toxicity tests using laboratory mice*

For the toxicity test 10 male adult laboratory mice (*Mus musculus*, BCA strain) weighting 20–35 g were randomly divided into two groups. For general anaesthesia the animals were treated by the 0.2 mg/ml solutions of xylazine, tiletamine and zolazepam, the hair was partially removed, the freed skin surface was disinfected by chlorhexidine, and the compound I in physiological solution with the quantity of 0.2 mg/kg was injected subcutaneously. The second group of mice remained the control group. After 14 days the mice were sacrificed, and the fresh blood samples were taken. The content of aspartate transaminase and alanine aminotransferase in the blood samples were estimated spectrophotometrically. The bodies were dissected, and the tissues were examined for inflammation, fibrosis, vascularisation, and neoplasm. The hearts and the livers were also weighted. For each group the average masses of mice, their hearts and livers, their standard deviations and confidence intervals ($f$ = 4, $p$ = 0.95) were estimated. The

results of both groups were compared using the Wilcoxon signed rank test.

*Spectrophotometric determination of aspartate transaminase and alanine aminotransferase in laboratory mice blood serum*

The concentration of the liver enzymes in the samples of mice blood serum was determined according to the method described in work [77] using the commercially available assay kits (B 01.05 and B 02.05, Vital LLC, Russia). The determination of alanine aminotransferase is based on the enzyme-catalysed transformation of L-alanine and α-ketoglutarate into pyruvic acid and L-glutamate with subsequent oxidation of nicotinamide adenine dinucleotide by formed pyruvic acid with the help of the enzyme lactate dehydrogenase. A reagent in the kit (B 01.05, Vital LLC, Russia) contained the solutions of 400 mmol/l L-alanine, 75 mmol/l Tris-HCl buffer, 1040 U/l lactate dehydrogenase, 3 mmol/l α-ketoglutarate and 0.036 mmol/l NADH. Freshly taken mice blood samples were centrifuged over 15 min at 3000 rpm, 0.2 ml of obtained serum was mixed with 2.0 ml of the reagent, incubated at 37°C, and the absorbance of the resulting solution at 340 nm against distilled water was registered in quartz cuvette with optical path length of 1 cm over 3 minutes. The activity of alanine aminotransferase in U/l was calculated from the rate of absorbance decrease as 1746 . dA/dt. A unit activity of the enzyme corresponds to catalysed transformation of 16.67 nmol/s of L-alanine.

The determination of aspartate transaminase is based on the enzyme-catalysed transformation of L-aspartate and α-ketoglutarate into oxaloacetate and L-glutamate with subsequent oxidation of nicotinamide adenine dinucleotide by formed oxaloacetate with the help of the enzyme malate dehydrogenase. A reagent in the kit (B 02.05, Vital LLC, Russia) contained the solutions of 192 mmol/l L-aspartate, 64 mmol/l Tris-HCl buffer, 480 U/l lactate dehydrogenase, 480 U/l malate dehydrogenase, 2.4 mmol/l α-ketoglutarate and 0.036 mmol/l NADH. Again, 0.2 ml of obtained serum was mixed with 2.0 ml of the reagent, incubated at 37 oC, and the absorbance of the resulting solution at 340 nm against distilled water was registered in quartz cuvette with optical path length of 1 cm over 3 minutes. The activity of aspartate transaminase in U/l was calculated from the rate of absorbance decrease as 1746 . dA/dt. A unit activity of the enzyme corresponds to catalysed transformation of 16.67 nmol/s of L-aspartate.

The analytical performance of both test kits as stated by manufacturer is as follows: linearity range 10 – 190 U/l, LOQ 7 U/l, relative uncertainty and relative standard deviation less than 5%.

For each group the average values of enzyme activities, their standard deviations and confidence intervals (f = 4, p = 0.95) were estimated. The results of both groups were compared using the Wilcoxon signed rank test.

## Results and discussion

*$^1$H NMR spectroscopy*

The experimental $^1$H NMR spectrum of compound I recorded at 400MHz in CDCl3 revealed the following bands: 12.74 (1H, Ar-OH), 8.76 (1H, Ar-CH=N-), 8.57-7.00 (7H, Ar-H). For comparison, the model NMR spectrum of this compound predicted by the online tool nmrdb.org [78] revealed the bands 6.88 (1H), 7.37 (1H), 7.46-7.66 (2H), 7.91 (1H), 8.48 (1H), 8.62 (1H), 8.90 (1H). As one might see, the experimental and predicted spectra coincide well.

*Crystal structure and Hirshfeld surface analysis*

The formulae and schemas of tautomeric transformations of the compound **I** are presented in Figure 1. In accordance with the data of monocrystal X-ray difractometry (CCDC number 1869718 [60]), the compound **I** crystallises in monoclinic singony, a space group $P2_1/n$. The cell parameters: a = 4.5628 Å, b = 19.3486 Å, c = 12.0485 Å, α = 90°, β = 95.27, γ = 90°, Z = 4 [61]. The compound **I** in its crystalline state is predominantly represented by the enolimine form. The structure is characterised by an intermolecular hydrogen bond O11–H12···N15 (bond length O11–H12 equals 0.90(3) Å, bond length H12···N15 equals 1.84(3) Å, angle O11–H12···N15 equals 145(3)°). The geometric structure of enolimine, *cis*-ketoenamine and *trans*-ketoenamine forms obtained by using the B3LYP/6-311++G(d,p) method is presented in Figure 2.

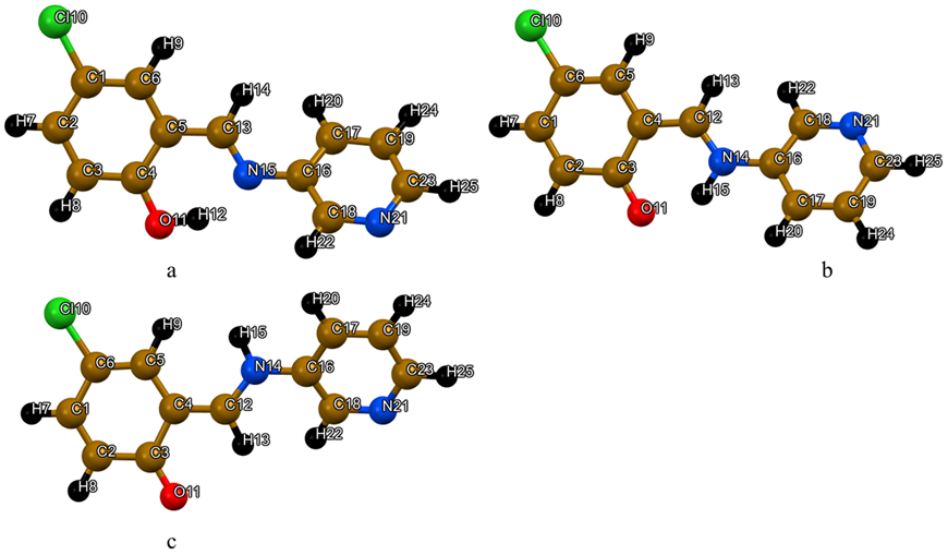


**Figure 2 –** Molecular structure of compound **I** tautomeric forms obtained by B3LYP/6-311++G(d,p) method (a – enolimine, b – *cis*-ketoenamine c – *trans*-ketoenamine)

**Table 1 –** Selected bond lengths (Å) and angles (°) in the experimental structure of I [47] and optimized structure of enol-imine form of I using the B3LYP/6-311++G(d,p) method

| | Experimental [47] | Calculated | | Experimental [47] | Calculated |
|---|---|---|---|---|---|
| *Bond lengths* | | | | | |
| C1–C2 | 1.388(3) | 1.398 | C19–C23 | 1.378(3) | 1.393 |
| C1–C6 | 1.374(2) | 1.382 | C16–C18 | 1.394(2) | 1.403 |
| C2–C3 | 1.370(3) | 1.388 | C1–Cl10 | 1.742(2) | 1.764 |
| C3–C4 | 1.391(3) | 1.399 | C4–O11 | 1.352(2) | 1.345 |
| C4–C5 | 1.409(2) | 1.418 | O11–H12 | 0.900(3) | 0.997 |
| C5–C6 | 1.402(2) | 1.407 | N11–C12 | 1.478(5) | 1.472 |
| C5–C13 | 1.449(2) | 1.452 | C13–N15 | 1.279(2) | 1.288 |
| C12–C13 | 1.516(6) | 1.537 | N15–C16 | 1.418(2) | 1.407 |
| C16–C17 | 1.394(2) | 1.399 | C23–N21 | 1.333(3) | 1.340 |
| C17–C19 | 1.379(3) | 1.389 | N21–C18 | 1.336(3) | 1.333 |
| *Bond angles* | | | | | |
| C1–C2–C3 | 119.6(2) | 120.8 | C2–C1–Cl10 | 119.2(1) | 119.4 |
| C2–C3–C4 | 120.9(2) | 120.5 | C3–C4–O11 | 119.0(1) | 118.7 |
| C3–C4–C5 | 119.6(2) | 119.5 | C4–O11–H12 | 111.0(2) | 107.3 |
| C4–C5–C6 | 118.8(1) | 119.3 | C13–N15–C16 | 121.5(1) | 121.4 |
| C1–C6–C5 | 120.1(2) | 120.4 | N15–C16–C18 | 118.2(1) | 117.8 |
| C6–C5–C13 | 119.4(1) | 119.2 | C19–C23–N21 | 122.8(2) | 123.0 |
| C16–C17–C19 | 119.5(2) | 118.7 | C18–N21–C23 | 117.5(2) | 117.8 |
| C17–C19–C23 | 117.1(2) | 117.8 | C16–C18–N21 | 124.0(2) | 123.7 |
| C17–C16–C18 | 118.4(4) | 117.8 | | | |
| *Dihedral angles* | | | | | |
| C1–C2–C3–C4 | –0.6(8) | –0.1 | C6–C5–C13–N15 | –2.2(2) | –0.23 |
| C2–C3–C4–C5 | 1.8(3) | 0.1 | C5–C13–N15–C16 | 179.1(1) | 177.6 |

*Continuation of the table*

| | Experimental [47] | Calculated | | Experimental [47] | Calculated |
|---|---|---|---|---|---|
| C3–C4–C5–C6 | –1.7(2) | 0.1 | C13–N15–C16–C17 | 2.3(3) | –34.0 |
| C4–C5–C6–C1 | –0.5(2) | –0.1 | N15–C16–C17–C19 | –179.2(2) | –179.1 |
| C2–C1–C6–C5 | 0.6(3) | 0.1 | C16–C17–C19–C23 | 0.2(3) | 0.5 |
| C6–C1–C2–C3 | –0.7(3) | 0.0 | C18–N21–C23–C19 | –0.6(3) | –0.2 |
| C3–C4–O11–H12 | –179.2(2) | –179.4 | C16–C18–N21–C23 | –0.2(3) | –1.0 |
| Cl10–C1–C2–C3 | –179.9(1) | –179.9 | | | |

Generally, a good agreement between the experimental and calculated values of bond lengths, bond angles and dihedral angles for enolimine form of **I** (Table 1) is observed. Thus, the differences between the bond lengths are about 0.01 Å. A notable exception is the dihedral angle C13–N15–C16–C17, which value according to the experimental data is about 2°. The calculated dihedral angle C13–N15–C16–C17 equals 34°. A similar picture is observed in the paper [47]. A possible explanation of this phenomenon might be the presence of the network of intermolecular interactions in the crystal structure that makes the molecule **I** flat. The geometric parameters of both *cis*- and *trans*-ketoenamine forms obtained by using the B3LYP/6-311++G(d,p) method are listed in Table S2.

In order to obtain additional information on intermolecular interactions in the crystal structure of compound **I** a Hirshfeld surface, including 2D fingerprints of interatomic contacts, was generated and studied. The model data were obtained using a CrystalExplorer 17 software. In addition to the 2D fingerprints the the enrichment ratios (*E*) of the intermolecular contacts were estimated in order to determine the contributions of different elements to the intermolecular interactions [79]. The appearance of the Hirshfeld surface of the compound **I** on the parameters denote normalised distance $d_{norm}$, shape index and curvedness is presented in Figure 3. The red areas on the $d_{norm}$ surfaces depict the presence of intermolecular hydrogen bonds C–H···O and C–H···N. The donors and the acceptors in the frameworks of corresponding interactions are presented on the shape index surface.

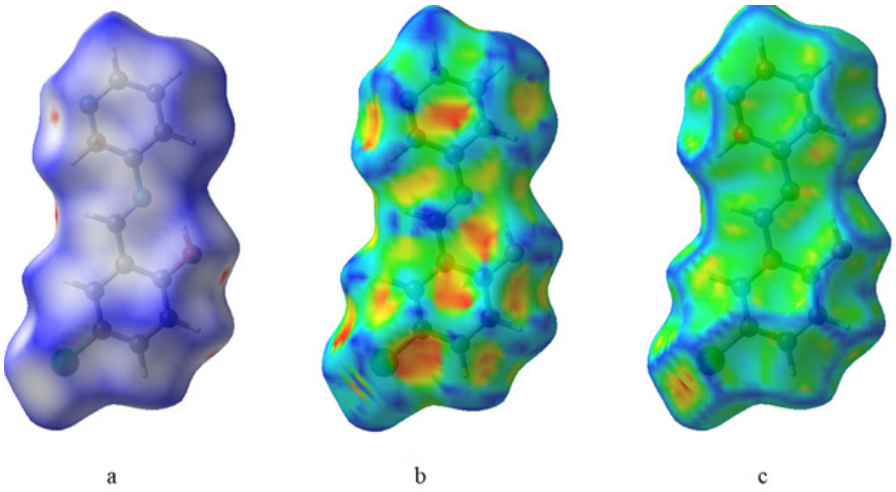


**Figure 3** – Molecular Hirshfeld surfaces of form II of tautomeric forms of compound **I** obtained by B3LYP/6-311++G(d,p) method (a – normalized distance $d_{norm}$, b – shape index, c – curvedness)

Figure 4 presents 2D fingerprint plots for all atoms participating in intermolecular interactions, as well as for atomic pairs H···X (X = H, C, N, O, Cl). Paired contacts H···N and H···O on the 2D fingerprint plots have the form of keen pikes with the heights at di ≈ 1.1, de ≈ 0.7 (di ≈ 0.7, de ≈ 1.1, total 1.8 nm) and

di ≈ 1.0, de ≈ 0.7 (di ≈ 0.7, de ≈ 1.0, total 1.7 nm). These contacts correspond to the hydrogen bonds C–H···O and C–H···N. The similar sums (or minimal distances between atoms) for other paired contacts equal: H···H – 1.4 nm, H···C – 2.2 nm, H···Cl – 2.2 nm, C···C – 2.6 nm, and C···N – 2.7 nm. The mutual contacts C···C, H···O and H···Cl, C···N, Cl···Cl are preferred for the structure of the compound **I**, because the enrichment ratio values for these paired mutual contacts exceed unity (Table 2). The contacts of hydrogen atoms are somewhat less preferable (E = 0.92), this could be explained by the largest proportion of the surface occupied by hydrogen, carbon and chlorine atoms.

The distribution of intermolecular interaction energies relative to the central molecule was calculated using the method B3LYP/6-31G(d,p). The calculation results are listed Table 3, and the visualisation of the interacting molecules is presented in Figure 5. It was revealed that the largest contribution to the total interaction energy was made by the dispersive interactions. This is mostly typical for molecules packed parallel to each other along the planes of aromatic rings. (Table 3, Figure 5). For such molecules, the dispersion interaction energy equals 62 kJ/mol. The strongest electrostatic interactions (10.5 kJ/mol) apparently correspond to hydrogen bonds C–H···O and C–H···N.

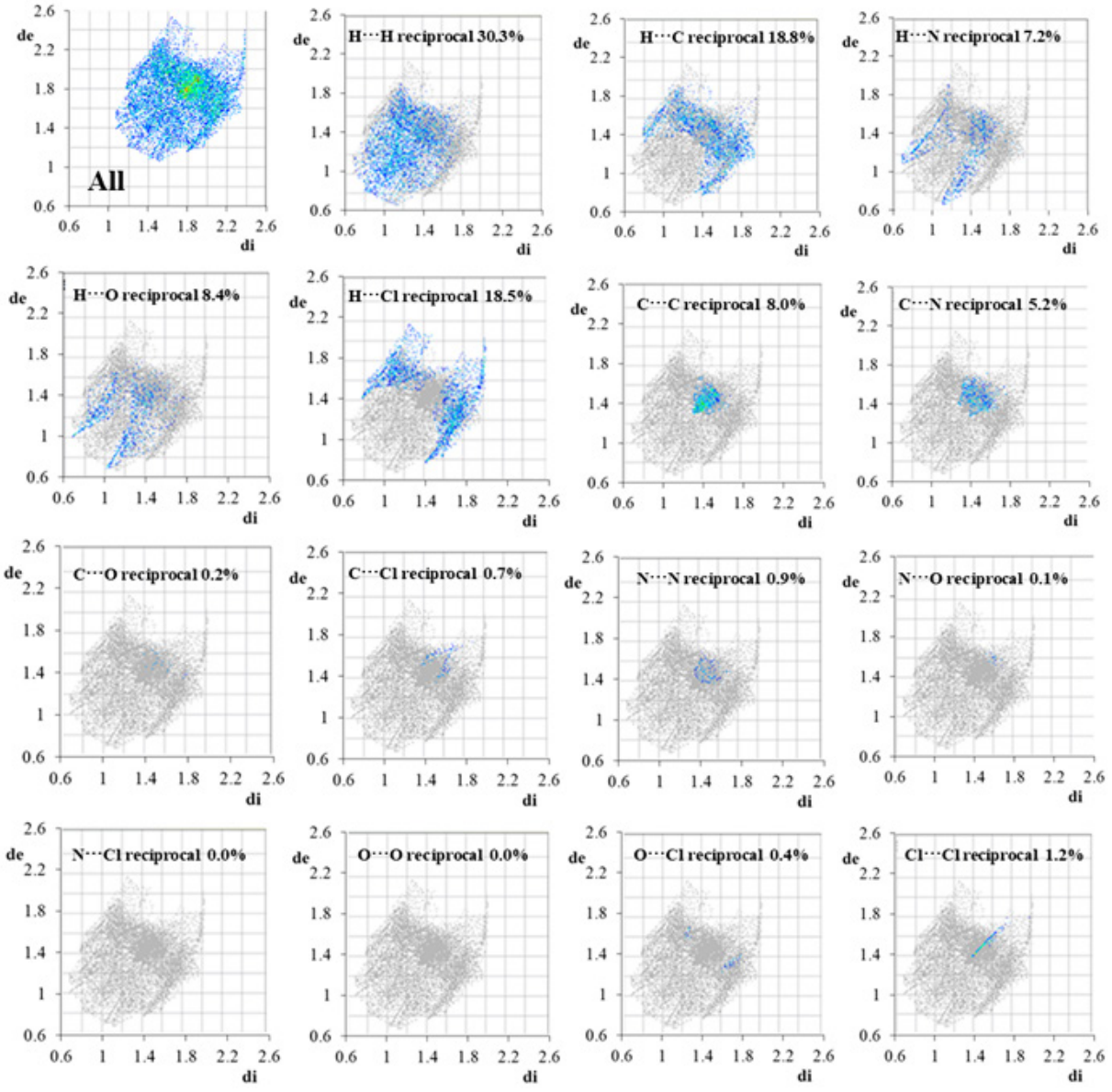


**Figure 4 –** Total 2D and decomposed 2D fingerprint plots of observed contacts for compound **I** crystal structure

**Table 2 –** Hirshfeld contact surface and it characteristics for compound **I**

| | H | C | N | O | Cl |
|---|---|---|---|---|---|
| Contacts (*C*, %)[a] | | | | | |
| H | 30.3 | – | – | – | – |
| C | 18.8 | 8.0 | – | – | – |
| N | 7.2 | 5.2 | 0.9 | – | – |
| O | 8.4 | 0.2 | 0.1 | 0.0 | – |
| Cl | 18.5 | 0.7 | 0.0 | 0.4 | 1.2 |
| Surface (*S*, %) | | | | | |
| | 56.8 | 20.5 | 7.2 | 4.5 | 11.0 |
| Random contacts (*R*, %) | | | | | |
| H | 32.3 | – | – | – | – |
| C | 23.2 | 4.2 | – | – | – |
| N | 8.2 | 3.0 | 0.5 | – | – |
| O | 5.2 | 1.8 | 0.5 | 0.2 | – |
| Cl | 12.5 | 4.6 | 1.6 | 1.0 | 1.2 |
| Enrichment (*E*)[b] | | | | | |
| H | 0.93 | – | – | – | – |
| C | 0.81 | 1.90 | – | – | – |
| N | 0.88 | 1.73 | – | – | – |
| O | 1.62 | 0.11 | – | – | – |
| Cl | 1.48 | 0.15 | 0.00 | 0.40 | 1.00 |

[a]Values are obtained from CrystalExplorer 17. [b]The "enrichment ratios" were not computed when the "random contacts" were lower than 0.9%, as they are not meaningful.

**Table 3 –** Interaction energies (kJ/mol) calculated with the B3LYP/6-31G(d,p) energy model for the crystal structure of compound **I**

| | No | Symmetry operation | R | E_ele | E_pol | E_dis | E_rep | E_tot |
|---|---|---|---|---|---|---|---|---|
| | 2 | x, y, z | 4.56 | -8.7 | -1.2 | -61.7 | 35.1 | -42.1 |
| | 2 | -x+1/2, y+1/2, -z+1/2 | 9.97 | -2.7 | -0.4 | -8.7 | 4.7 | -7.8 |
| | 2 | x+1/2, -y+1/2, z+1/2 | 9.55 | -1.1 | -0.1 | -4.4 | 1.5 | -4.1 |
| | 2 | x+1/2, -y+1/2, z+1/2 | 8.72 | -6.4 | -1.7 | -9.9 | 9.4 | -10.9 |
| | 2 | x+1/2, -y+1/2, z+1/2 | 6.28 | -10.5 | -2.7 | -17.3 | 14.4 | -19.3 |
| | 2 | x+1/2, -y+1/2, z+1/2 | 6.67 | -2.6 | -1.1 | -12.7 | 7.7 | -9.9 |
| | 1 | -x, -y, -z | 12.13 | -2.5 | -0.2 | -3.9 | 0.0 | -6.1 |
| | 2 | -x+1/2, y+1/2, -z+1/2 | 10.20 | -2.0 | -0.6 | -11.9 | 7.1 | -8.6 |
| | 1 | -x, -y, -z | 11.00 | 1.5 | -0.7 | -8.4 | 2.4 | -4.7 |

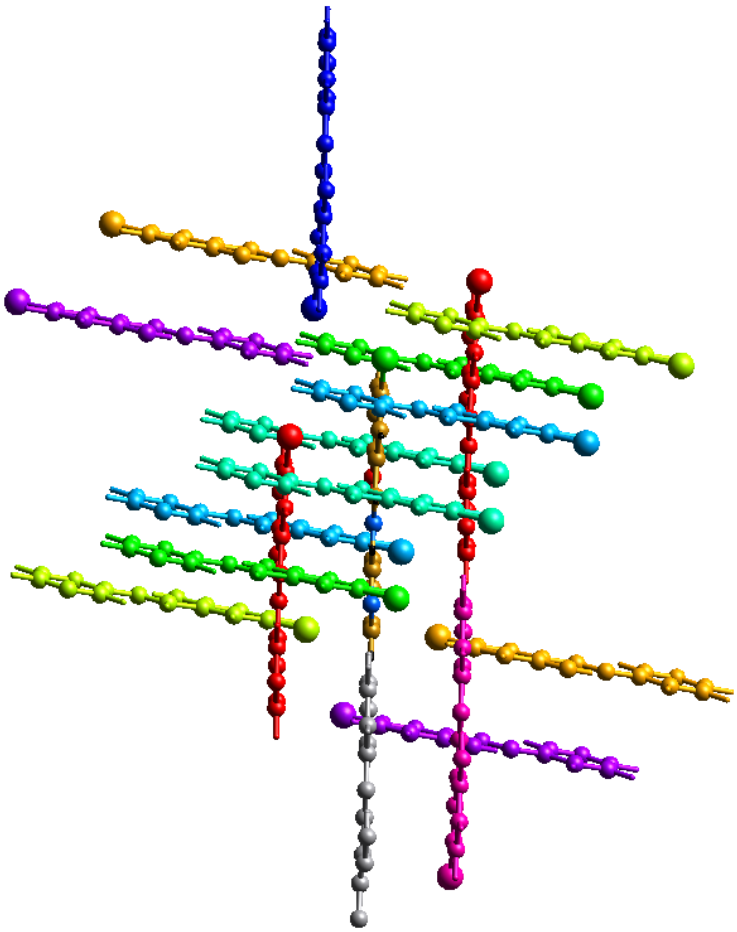

**Figure 5 –** The color-coded interaction mapping within 3.8 Å of the centering molecule in the crystal structure of compound **I**, calculated with the B3LYP/6-31G(d,p) energy model

*Vibrational analysis*

To calculate the vibration frequencies appearing in IR spectra for both enolimine, *cis*-, and *trans*-ketoenamine forms of the compound **I**, a DFT method was used. The experimental and predicted IR spectra are presented in Figure 6.

It is well known that the predicted wavenumbers of vibrational bands are usually some higher than the experimental ones. [80]. This fact was taken into account while interpreting the absorption bands in the experimental spectrum and their comparison with the bands of calculated spectra. It is important to note that the comparison of the experimental and calculated bands in the range from 4000 to 1700 $cm^{-1}$ was not conducted, because the position of bands corresponding to valence oscillations of hydroxyl groups located in this region is heavily influenced by intermolecular interactions in the crystal structure, including C–H···O and C–H···N. Thus in the experimental spectrum there is a broad peak related to hydroxyl groups with the maximum at 3430 $cm^{-1}$, and in the calculated spectra an analogous high intensity band is present at 3143 $cm^{-1}$. Table 4 provides a decoding of vibrational modes and a comparison of the frequencies of calculated and experimental vibrations. Coinciding frequencies are highlighted in bold, taking into account the reduction factor of 1.021457 for calculated frequencies. As expected, the match was best for the enolimine form, which gives another confirmation of its prevalence in crystalline state of compound **I**. The vibrational modes for *cis*- and *trans*-ketoenamine forms of compound **I** are listed in Tables S3 and S4.

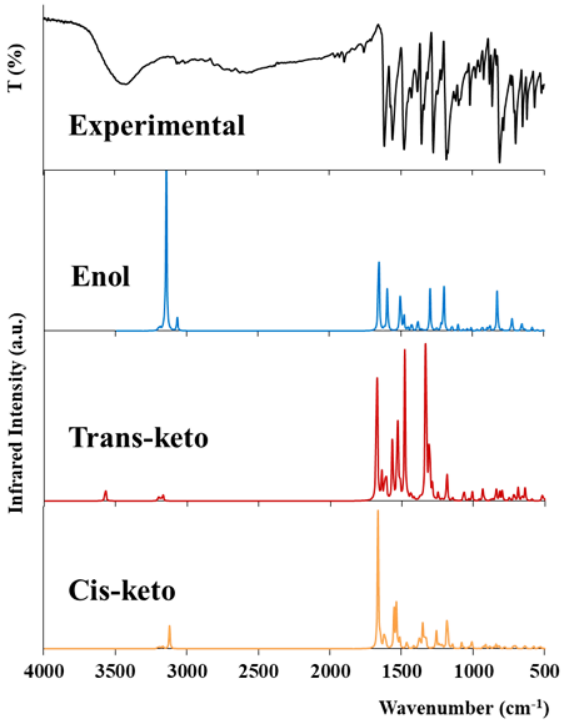


**Figure 6 –** The experimental IR spectrum of compound **I** in solid state, and calculated IR spectra of its different tautomeric forms

**Table 4 –** The vibration modes in the calculated IR spectrum (Figure 7) of the ground state of enol-imine form of compound **I** and the peaks of the experimental IR spectrum

| Calculated molecular vibration (PED, %)[a] | Calculated frequency ($cm^{-1}$) | Calculated intensity ($km \cdot mol^{-1}$) | Experimental frequency ($cm^{-1}$)/ Intensity |
|---|---|---|---|
| *ν*O11–H12 (100) | 3206 | 1.89 | 3425/ Medium |
| *ν*C17–H20 + *ν*C19–H24 (100) | 3198 | 10.99 | 3067/ Low |
| *ν*C2–H7 + *ν*C3–H8 (13); *ν*C6–H9 (87) | 3194 | 0.35 | 3050/ Low |
| *ν*C2–H7 + *ν*C3–H8 (87); *ν*C6–H9 (13) | 3192 | 6.54 | 3008/ Low |
| *ν*C17–H20 (100) | 3184 | 14.02 | 2989/ Low |
| *ν*C23–H25 (87); *ν*C18–H22 + *ν*C23–H25 (13) | 3164 | 9.50 | 2971/ Low |
| *ν*C23–H25 (13); *ν*C18–H22 + *ν*C23–H25 (87) | 3157 | 15.44 | 1959/ Low |
| *ν*O11–H12 (97) | 3143 | 944.21 | 1929/ Low |
| *ν*C13–H14 (98) | 3067 | 81.69 | 1896/ Low |
| | | | 1818/ Low |
| | | | 1758/ Low |
| *ν*N15–C13 + *ν*C1–C6+ *ν*C3–C4 + *ν*C1–C2 + *ν*C2–C3 (53) | **1657** | **207.79** | **1617/High** |
| *ν*N15–C13 + *ν*C1–C6+ *ν*C3–C4 + *ν*C19–C23 + *ν*C2–C3 (50) | 1653 | 31.34 | Not detected |
| *ν*C2–C3+ *ν*C5–C6 + *ν*C1–C6 + *ν*C3–C4 + *ν*N21–C18 *ν*N21–C23 (11); *ν*C17–C19 + *ν*C5–C6 (39) | **1615** | **13.75** | **1572/ Low** |
| *ν*C16–C17 + *ν*C19–C23 (53) | 1600 | 11.97 | Not detected |
| *ν*N15–C13 + *ν*C5–C6+ *ν*C1–C2 (50); *β*H12–O11–C4 (12); *β*H7–C2–C3 + *β*H8–C3–C4 + *β*H9–C6–C5 (10) | **1594** | **249.11** | **1555/ High** |

*Continuation of the table*

| Calculated molecular vibration (PED, %)[a] | Calculated frequency ($cm^{-1}$) | Calculated intensity ($km \cdot mol^{-1}$) | Experimental frequency ($cm^{-1}$)/ Intensity |
|---|---|---|---|
| *β*H12–O11–C4 (19); *β*H9–C6–C5 + *β*H8–C3–C4 + *β*H7–C2–C3 (16) | **1506** | **1701.20** | **1479/ High** |
| *ν*C17–C19 + *ν*N21–C18+ *ν*N21–C23 (14); *β*H9–C6–C5 (12) + *β*H8–C3–C4 + *β*H7–C2–C3 (15); *β*H20–C17–C19 + *β*H22–C18–N21 + *β*H25–C23–N21 (11); *β*H22–C18–N21 + *β*H25–C23–N21 + *β*H14–C13–N15 (20) | **1500** | **99.36** | **1450/ Medium** |
| *β*H12–O11–C4 (12); *β*H9–C6–C5 + *β*H8–C3–C4 + *β*H7–C2–C3 (17); *β*C1–C2–C3 + *β*C2–C1–C6 + *β*C2–C3–C4 (10) | **1478** | **92.58** | **1435/ Medium** |
| *β*H12–O11–C4 (10); *β*H22–C18–N21 + *β*H25–C23–N21 + *β*H14–C13–N15 + *β*H24–C19–N23 (31) | 1451 | 23.48 | Not detected |
| *ν*C2–C3+ *ν*C5–C6 + *ν*C1–C6 + *ν*C3–C4 + *ν*N21–C18 + *ν*N21–C23 (22); *β*H12–O11–C4 (11); *β*H14–C13–N15 + *β*H9–C6–C5 + *β*H25–C23–N21 + *β*H8–C3–C4 (18) | **1424** | **52.28** | **1384/ Medium** |
| *β*H14–C13–N15 + *β*H9–C6–C5 + *β*H22–C81–N21 + *β*H25–C23–N21 (57) | **1381** | **72.07** | **1355/ High** |
| *β*H20–C17–C19 + *β*H22–C18–N21 + *β*H25–C23–N21 + *β*H24–C19–C23 (65) | **1356** | **10.45** | **1338/ Medium** |
| *ν*C1–C6+ *ν*C1–C2 + *ν*C5–C13 (64) | **1340** | **5.11** | **1314/ Low** |
| *ν*O11–C4+ *ν*C5–C13 + *ν*C3–C4 (40); *β*H14–C13–N15 + *β*H9–C6–C5 + *β*H25–C23–N21 + *β*H8–C3–C4 (12) | **1295** | **231.18** | **1274/ High** |
| *ν*N21–C18+ *ν*N21–C23 + *ν*C19–C23 (63) | 1283 | 5.65 | |
| *ν*N15–C16 (10); *β*H14–C13–N15 + *β*H9–C6–C5 + *β*H25–C23–N21 + *β*H8–C3–C4 (24) | **1259** | **2.42** | **1243/ Medium** |
| *ν*N15–C16 (19); *ν*C5–C13+ *ν*C3–C4 + *ν*N15–C16 (13); *β*H14–C13–N15 + *β*H9–C6–C5 + *β*H25–C23–N21 + *β*H8–C3–C4 (12); *β*H22–C18–N21 + *β*H25–C23–N21 + *β*H14–C13–N15 (10) | **1249** | **18.26** | **1219/ Low** |
| *ν*C17–C19 + *ν*N21–C18+ *ν*N21–C23 (12); *β*H22–C18–N21 + *β*H25–C23–N21 + *β*H14–C13–N15 + *β*H24–C19–N23 (11); *β*H22–C18–N21 + *β*H25–C23–N21 + *β*H14–C13–N15 (23) | 1218 | 32.63 | Not detected |
| *ν*C5–C13+ *ν*C3–C4 + *ν*N15–C16 (32) | **1199** | **293.30** | **1170/ High** |
| *ν*C2–C3+ *ν*C5–C6 + *ν*C1–C6 + *ν*C3–C4 + *ν*N21–C18 + *ν*N21–C23 (16); *β*H7–C2–C3 + *β*H8–C3–C4 + *β*H9–C6–C5 (47) | **1147** | **9.89** | **1125/ Medium** |
| *ν*C17–C19 + *ν*N21–C18+ *ν*N21–C23 (26); *β*H20–C17–C19 + *β*H24–C19–C23 (51) | 1139 | 22.60 | Not detected |
| *ν*C1–C2 + *ν*C2–C3 (39); *ν*Cl10–C1 (11); *β*H9–C6–C5 + *β*H8–C3–C4 + *β*H7–C2–C3 (26) | **1100** | **36.46** | **1080/ Medium** |
| *ν*C19–C23 + *ν*N21–C23+ C17–C19 (54); *β*H22–C18–N21 + *β*H25–C23–N21 + *β*H14–C13–N15 + *β*H24–C19–N23 (10) | **1062** | **9.97** | **1037/ Low** |
| *β*C18–N21–C23 + *β*C17–C19–C23 + *β*C19–C23–N21 (72) | **1034** | **14.83** | **1010/ Medium** |
| *τ*H14–C13–N15–C16 (82) | 1009 | 17.85 | |
| *τ*H24–C19–C23–N21 (70) | **1004** | **0.36** | **975/ Low** |
| *τ*H7–C2–C3–C4 + *τ*H8–C3–C4–C5 (72) | **969** | **1.49** | **954/ Low** |
| *τ*H20–C17–C19–C23 + *τ*H22–C18–N21–C23 + *τ*H25–C23–N21–C18 (72) | 965 | 7.50 | Not detected |

*Continuation of the table*

| Calculated molecular vibration (PED, %)[a] | Calculated frequency ($cm^{-1}$) | Calculated intensity ($km \cdot mol^{-1}$) | Experimental frequency ($cm^{-1}$)/ Intensity |
|---|---|---|---|
| τH22–C18–N21–C23 + τH25–C23–N21–C18 (66); τC17–C19–C23–N21 + τC18–N21–C23–C19 (66) | **938** | **5.19** | **923/ Medium** |
| τH9–C6–C5–C4 (72); τC1–C6–C5–C13 (10) | **894** | **19.21** | **880/ Medium** |
| νN15–C16 (10); βC19–C23–N21 + βC5–C13–N15 + βC1–C2–C3 + βC18–N21–C23 + βC16–C17–C19 (44) | **877** | **33.61** | **861/ Medium** |
| τH12–O11–C4–C3 (40); τH7–C2–C3–C4 + τH8–C3–C4–C5 (45) | **845** | **1.87** | **830/ Low** |
| τH12–O11–C4–C3 (51); τH7–C2–C3–C4 + τH8–C3–C4–C5 (25) | **825** | **210.86** | **805/ High** |
| τH24–C19–C23–N21 (58) | 823 | 31.11 | Not detected |
| νC1–C2 + νC2–C3 (14); νO11–C4 (12); βC1–C2–C3 + βC2–C1–C6 + βC2–C3–C4 (22) | **791** | **7.9** | **787/ Medium** |
| τH9–C6–C5–C4 (11); τH7–C2–C3–C4 + τH8–C3–C4–C5 (10); τH7–C2–C3–C4 + τH8–C3–C4–C5 (13); τC1–C6–C5–C13 + τC1–C2–C3–C4 + τC3–C2–C1–C6 + τC2–C1–C6–C5 (10); out-of-planeO11–C3–C5–C4 (29) | **737** | **2.91** | **726/ Low** |
| βC5–C13–N15 + βC6–C15–C13 + βC19–C23–N21 + βC17–C19–C23 (28); τC18–N21–C23–C19 + τC16–C17–C19–C23 (14) | **723** | **62.49** | **710/ Low** |
| βC5–C13–N15 + βC6–C15–C13 + βC19–C23–N21 + βC17–C19–C23 (17); τH22–C18–N21–C23 + τH25–C23–N21–C18 (12); τC18–N21–C23–C19 + τC16–C17–C19–C23 (27) | **718** | **30.07** | **700/ High** |
| βC2–C3–C4 + βC1–C6–C5 + βC1–C2–C3 (40); νCl10–C1 (16); βC2–C1–C6 + βC1–C2–C3 + βC1–C6–C5 (11) | **654** | **53.39** | **646/ Medium** |
| βC18–N21–C23 + βC17–C19–C23 (72) | **634** | **15.58** | **622/ Medium** |
| βC2–C1–C6 + βC1–C2–C3 + βC1–C6–C5 (11); βC16–C17–C19 + βC6–C5–C13 (27) | **581** | **16.67** | **568/ Medium** |
| τC3–C2–C1–C6 + τC2–C1–C6–C5 (60) | 578 | 5.88 | Not detected |
| βC18–C16–N15 + βC13–N15–C16 + βC6–C15–C13 + βC16–C1z7–C19 (16); out-of-planeN15–C17–C18–C16 + τC2–C1–C6–C5 (35) | **543** | **7.97** | **520/ Low** |
| βC18–C16–N15 + βC13–N15–C16 + βC6–C15–C13 + βC16–C17–C19 (33); τC1–C6–C5–C13 (10); out-of-planeN15–C17–C18–C16 + τC2–C1–C6–C5 (15) | 504 | 4.85 | 516/ Low |

*Global reactivity descriptors and molecular orbitals*

In Table 5 the values of the global reactivity descriptors, calculated using B3LYP 6-311++G(d,p) for molecules in the gas phase are provided. A total energy is minimal for the enoimine form of the compound **I**. It is also worth noting the higher global chemical hardness of this form, which points the resistance of the electronic shell to deformation. Both of these parameters indicate the higher stability of the enolimine form. The highest occupied and the lowest unoccupied molecular orbitals for all three forms are localised mainly throughout the whole molecule (see Figure 7). The special features include localisation on the chlorine atom only for HOMO, as well as lower electron density of HOMO and LUMO on the nitrogen atom of the heterocycle.

**Table 5 –** Dipole moment, frontier molecular HOMO and LUMO orbitals and descriptors for three forms of compound **I** in gas phase, obtained by using the B3LYP/6-311++G(d,p) method

| Parameter | Enol form | *Cis*-keto form | *Trans*-keto form |
|---|---|---|---|
| Total energy (eV) | –30145.44228 | –30145.32565 | –30145.01196 |
| Dipole moment (Debye) | 3.89751 | 5.942917 | 8.738414 |
| $E_{HOMO}$ (eV) | –0.23729 | –0.22019 | –0.21759 |
| $E_{LUMO}$ (eV) | –0.08962 | –0.10001 | –0.10392 |
| $\Delta E_{LUMO-HOMO} = E_{LUMO} - E_{HOMO}$ (eV) | 0.14767 | 0.12018 | 0.11367 |
| Ionization energy, $I = -E_{HOMO}$ (eV) | 0.23729 | 0.22019 | 0.21759 |
| Electron affinity, $A = -E_{LUMO}$ (eV) | 0.08962 | 0.10001 | 0.10392 |
| Electronegativity, $\chi = (I + A)/2$ (eV) | 0.16346 | 0.16010 | 0.16076 |
| Chemical potential, $\mu = -\chi$ (eV) | –0.16346 | –0.16010 | –0.16076 |
| Global chemical hardness, $\eta = (I - A)/2$ (eV) | 0.07384 | 0.06009 | 0.05684 |
| Global chemical softness, $S = 1/(2\eta)$ ($eV^{-1}$) | 6.77186 | 8.32085 | 8.79740 |
| Global electrophilicity index, $\omega = \mu^2/(2\eta)$ (eV) | 0.18093 | 0.21328 | 0.22734 |
| Global nucleophilicity index, $E = \mu \times \eta$ ($eV^2$) | –0.01207 | –0.00962 | –0.00914 |

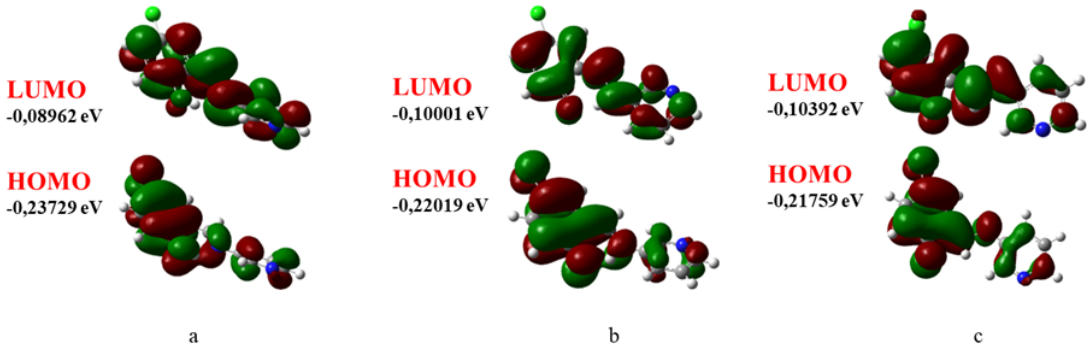


**Figure 7 –** Views on the electronic isosurfaces of LUMO and HOMO molecular orbitals of tautomeric forms of compound **I** obtained by using the B3LYP/6-311++G(d,p) method (a – enolimine, b – *cis*-keto-namine c – *trans*-ketoenamine; results under 0.02 a.u. isovalue)

The ionisation potential (I) and the affinity to electrons (A) were estimated as follows: I = −E (HOMO), A = −E (LUMO) [49]. Thus, a decrease in the values of I corresponds to an increase in electron-donating capacity, and an increase in A corresponds to an increase in electron-accepting capacity. For all forms of the compound **I** the ionisation energy lies in the range of 0.21 – 0.25 eV, and the affinity to electrons is about 0.1 eV. These values indicate more expressed electron donor ability of the compound.

For a general reactivity assessment, some additional characteristics calculated from the difference in the LUMO and HOMO energies, were also calculated [81]. Low electronegativity values (0.15 – 0.17 eV) also indicate the predominantly electron donor properties of the molecules.

*Molecular electrostatic potential surfaces*

The visualisation of electrophilic and nucleophilic centres of different forms of the compound **I** was carried out using molecular electrostatic potential (MEP) surfaces (see Figure 8).

The red and blue zones on the MEP surfaces depict nucleophilic and electrophilic centres respectively. As expected, the nucleophilic centres are the oxygen, nitrogen and chlorine atoms. For the enolimine form (Figure 8a) the nucleophilicities of oxygen and heterocyclic nitrogen are close to each other. For the ketoenamine forms (Figure 8b, c) this characteristic is far more pronounced for oxygen atom. The most pronounced electrophilic centre is the hydrogen at the carbon atom adjacent to the imine nitrogen.

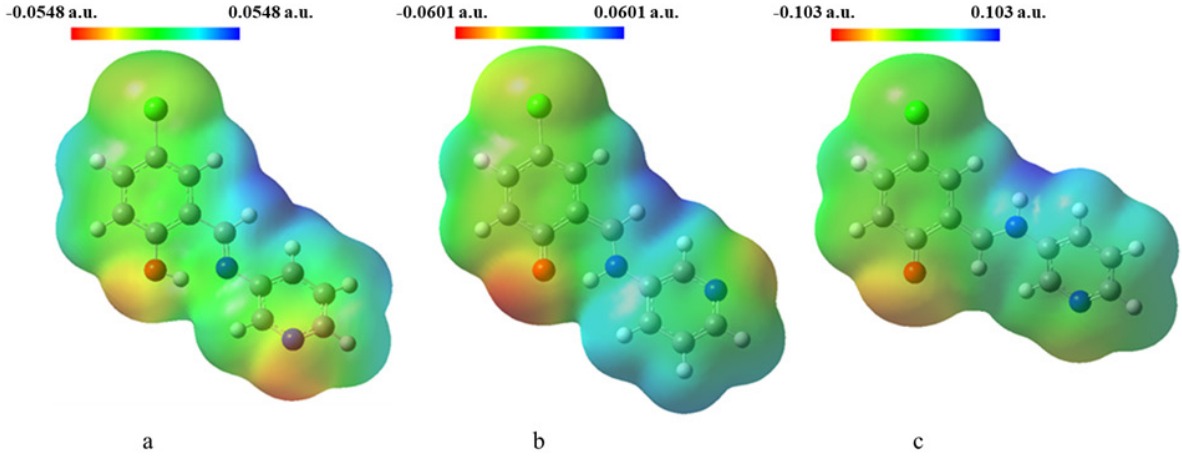


**Figure 8 –** View of the molecular electrostatic potential surfaces of compound **I**, obtained by using the B3LYP/6-311++G(d,p) method (a – enolimine, b – *cis*-keto-namine c – *trans*-ketoenamine; results under 0.004 a.u. isovalue)

*Absorption spectroscopy*

The calculated according to B3LYP 6-311++G(d,p) and the experimental UV-spectra of the compound **I** solution in ethanol are presented in Figure 9. The calculated spectra of the *cis*- and *trans*-ketoenamine forms of the compound **I** (Figures 9b, c) contain bands at 428 and 521 nm characteristic for these forms. The maxima of absorption band of enoimine form are located below 400 nm. A good agreement between the experimental spectrum (Figure 9d) and the calculated spectrum of enolimine form (Figure 9a) is observed. In the experimental and calculated spectra, the absorption maxima and bands at 357 and 355 nm; 301 and 312 nm; 210 and 224 nm closely coincide.

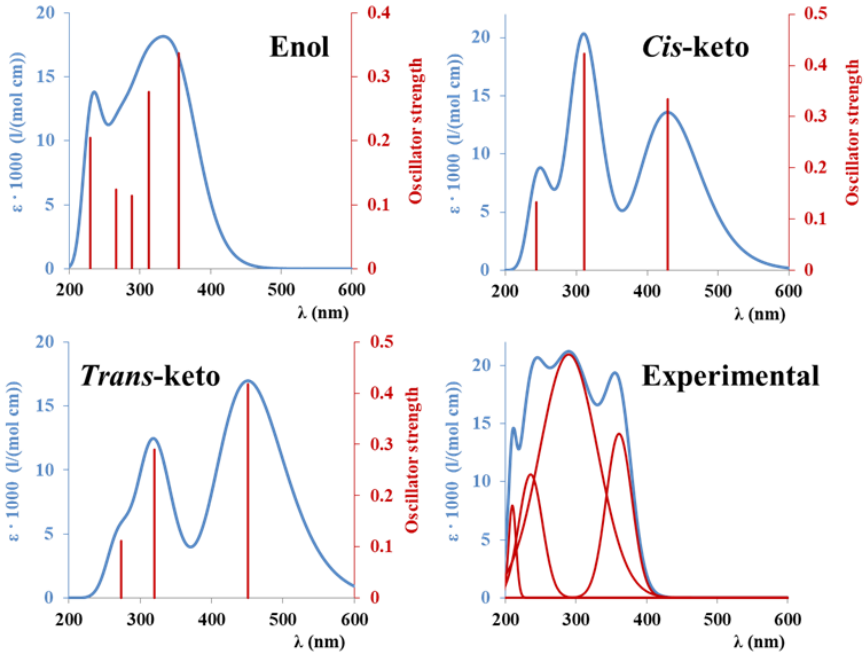


**Figure 9 –** The calculated absorption spectra of different tautomeric forms of compound **I** obtained by using the TD-DFT/B3LYP/6-311++G(d,p) method and experimental UV-vis spectrum of compound **I** in ethanol

The UV-spectra of the compound **I** in different both polar and non-polar solvents were also recorded and analysed for better understanding of the influence of medium on the tautomerism of this Schiff base. These spectra are presented in Figure 10. The UV-spectra in different alcohols are presented separately.

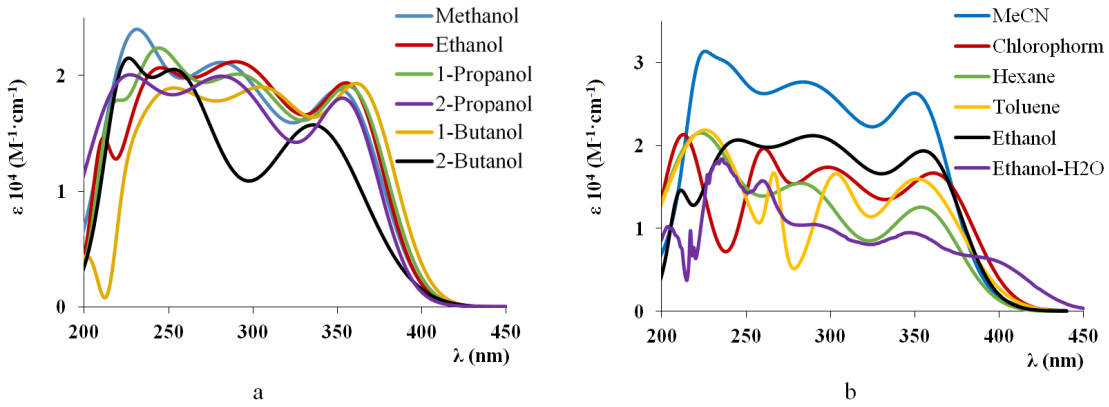


**Figure 10 –** Experimental UV-spectra of compound **I** in different solvents

The absorption bands corresponding to the π → π* and n → π* transitions are located in the ultraviolet region. The bands corresponding to the π→ π* transition in more polar solvents such as ethanol and chloroform are located at 209 and 215 nm correspondingly. A series of solvents sorted by the location of the longer wavelength band corresponding to the n → π* transition is as follows: toluene (351 nm) – hexane (352 nm) – acetonitrile (353 nm) – ethanol (357 nm) – chloroform (363 nm). Therefore, the increase of the solvent polarity apparently shifts the hydrogen atom from O11 toward N15. The spectrum of the compound **I** in the ethanol-water mixture containing 76 weight % ethanol is worth noting separately. An introduction of water somewhat shifts the position of the n→ π* transition band of enolimine form, but reveals a band at 400 nm, related with the ketoenamine form.

*Ionisation constants*

An oxygen-containing group and two nitrogen-containing groups are the acid-base centres in the structure of the compound **I**. Generally, the proteolytic equilibria of the compound **I** might be presented as follows [82]:

$$H_3A^{2+} \overset{K_1}{\rightleftharpoons} H_2A^{+} \overset{K_2}{\rightleftharpoons} HA \overset{K_3}{\rightleftharpoons} A^{-} \qquad (1)$$

The neutral form HA exists as the mixture of both enolimine and ketoenamine forms. The evaluation of the equilibrium constants of tautomeric transformations of the compound falls outside the scope of the present study. Only the acidity constants $K_1 - K_3$ are to be determined.

At the first step the UV-spectra of the compound **I** at different pH values in water-ethanolic mixtures with the 73 weight percent ethanol were recorded. The obtained spectra are presented in Figure 11a. There are several isosbestic points at 303, 361 and 364 nm. The absorbances of each solution at 390 nm were determined and plotted against the pH value (see Figure 11b). The jumps are present on the curve at the pH ranges 4.7 – 5.7 and 7.0 – 10.0. The potentiometric titration of the mixture was conducted (see Section 2.4) for more accurate analysis. The titration curve is presented in Figure 11c. The experimental curves were processed implementing the KEV algorithm [83] for estimation of ionic equilibrium constants. The obtained ionisation constant values are listed in Table 6. Apparently, $pK_{a1}$ corresponds to the dissociation of protonated pyridine nitrogen, $pK_{a2}$ – to the protonation of imine nitrogen, and $pK_{a3}$ – to the protonation of hydroxyl group [82].

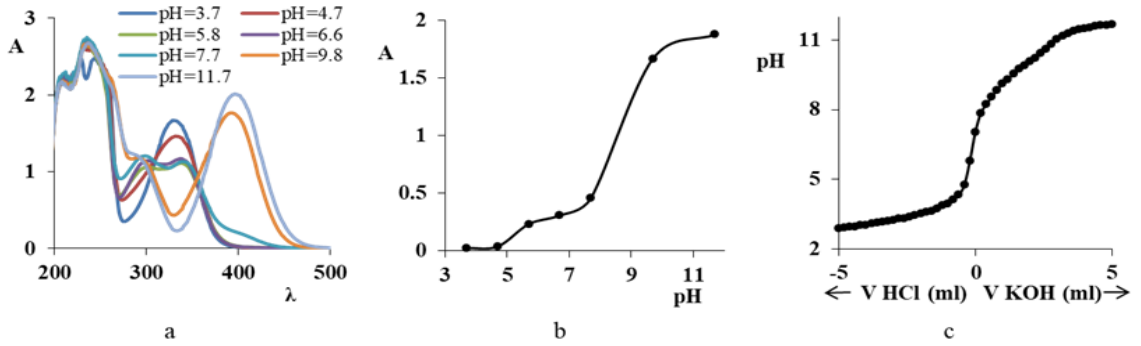


**Figure 11 –** UV-spectra of compound **I** in different pH (a), dependence of the absorption value on pH (b) and the titrimetric curve of compound **I** (c) in ethanol-water media (73% ethanol by weight)

**Table 6 –** Acidity constants of compound **I** in a water-ethanol mixture (73% ethanol by weight) obtained by potentiometric titration

| $pK_{a1}$ | $pK_{a2}$ | $pK_{a3}$ |
|---|---|---|
| 4.16 | 8.55 | 10.43 |

*Molecular docking*

To roughly estimate the level of binding energies of the compound **I** with target proteins, the molecular docking methodology was employed. The models of the structure of some proteins from the cell walls of *Staphylococcus aureus* (predominantly, sortase), factors of invasion LasA and LasB, hemolytic proteins LipA and LipB and Lasl protein of *Pseudomonas aeruginosa*, see Table 7. The original ligands (downloaded together with the protein structures from the PDB) were removed and the affinity calculation was performed for their binding sites. In the case of multiple original ligands, molecular docking was performed for the binding sites of each of them and the lowest affinity value obtained was recorded. In addition, the docking procedure for the known antibiotics azithromycin and ampicillin was performed on the same proteins.

**Table 7 –** Intermolecular interactions energies of gram-positive and gram-negative microorganisms proteins with original ligands, antibiotic molecules and tautomeric forms of **I**

| No | PDB code | Protein | Binding energy (kcal/mol) | | | | | |
|---|---|---|---|---|---|---|---|---|
| | | | Initial ligand[a] | Azithromycin | Ampicillin | Compound **I** | | |
| | | | | | | Enol form | *Cis*-keto form | *Trans*-keto form |
| Gram-positive bacteria proteins (*Staphylococcus aureus*) | | | | | | | | |
| 1 | 2KID | Sortase A with (PHQ) LPA(B27) peptide | –6.8 | –6.9 | –6.9 | –5.2 | –5.7 | –5.6 |
| 2 | 6R1V | Sortase A with 6-(hydroxymethyl)-3-oxidanyl-2-(thiophen-3-ylmethyl)pyran-4-one | –5.1 | –7.1 | –6.7 | **–5.7** | **–5.7** | **–5.7** |
| 3 | 4LFD | Sortase B with (CBZ) NPQ(B27) peptide | –6.9 | –7.6 | –7.4 | –6.5 | –6.5 | –6.5 |
| 4 | 1QXA | Sortase B with Gly3 | –4.6 | –7.6 | –6.4 | **–6.5** | **–6.4** | **–6.3** |
| 5 | 1QWZ | Sortase B | –4.7 | –7.6 | –7 | **–6.5** | **–6.6** | **–6.6** |
| 6 | 1QX6 | Sortase B with E64 | –5.7 | –8.1 | –7.1 | **–6.4** | **–6.5** | **–6.0** |
| Gram-negative bacteria proteins (mainly *Pseudomonas aeruginosa*) | | | | | | | | |
| 7 | 3IT7 | LasA elastase | –4,9 | –9.1 | –8.0 | **–6.5** | **–6.5** | **–6.5** |

*Continuation of the table*

| No | PDB code | Protein | Binding energy (kcal/mol) | | | | | |
|---|---|---|---|---|---|---|---|---|
| | | | Initial ligand[a] | Azithromycin | Ampicillin | Compound **I** | | |
| | | | | | | Enol form | *Cis*-keto form | *Trans*-keto form |
| 8 | 7NLM | LasB elastase | –5.8 | –7.4 | –7.0 | **–6.2** | **–6.0** | **–6.1** |
| 9 | 9G3R | LecA lectin with a synthetic thiogalactoside | –5,6 | –7,3 | –6.0 | –5.5 | –5.0 | –5.2 |
| 10 | 5A6Y | LecB lectin with mannose-alpha1,3mannoside | –6.0 | –6.2 | –5.6 | –5.2 | –5.1 | –5.2 |
| 11 | 1RO5 | AHL Synthase LasI | –4.6 | –8.9 | –7.0 | **–7.0** | **–6.9** | **–6.8** |

[a](from top to bottom) Initial ligand = (phenylmethyl) N-[(2S)-4-methyl-1-oxidanylidene-1-[(2S)-2-[[(2S)-1-oxidanylidene-1-[[(2S,3R)-3-oxidanyl-1-sulfanyl-butan-2-yl]amino]propan-2-yl]carbamoyl]pyrrolidin-1-yl]pentan-2-yl]carbamate; 6-(hydroxymethyl)-3-oxidanyl-2-(thiophen-3-ylmethyl)pyran-4-one; (phenylmethyl) N-[(2S)-4-azanyl-1-[(2S)-2-[[(2S)-5-azanyl-1,5-bis(oxidanylidene)-1-[[(2S,3R)-3-oxidanyl-1-sulfanyl-butan-2-yl]amino]pentan-2-yl]carbamoyl]pyrrolidin-1-yl]-1,4-bis(oxidanylidene)butan-2-yl] carbamate; trimethyl-(2-sulfanylethyl)azanium; trimethyl-(2-sulfanylethyl)azanium; [amino-[4-[[(2S)-2-[[(2S)-2,4-dihydroxy-4-oxo-butanoyl]amino]-4-methyl-pentanoyl]amino]butylamino]methylidene]azanium; (2R,3R)-2,3-dihydroxybutanedioic acid and propane-1,2,3-triol; (S)-2-mercapto-N-(4-methoxyphenyl)-4-methylpentanamide; (2R,3R,4S,5R,6S)-2-(hydroxymethyl)-6-sulfanyl-oxane-3,4,5-triol and 2-(2-hydroxyethyloxy)ethanol; (2S,3S,4S,5S,6R)-6-(hydroxymethyl)oxane-2,3,4,5-tetrol and propane-1,2,3-triol; sulfate.

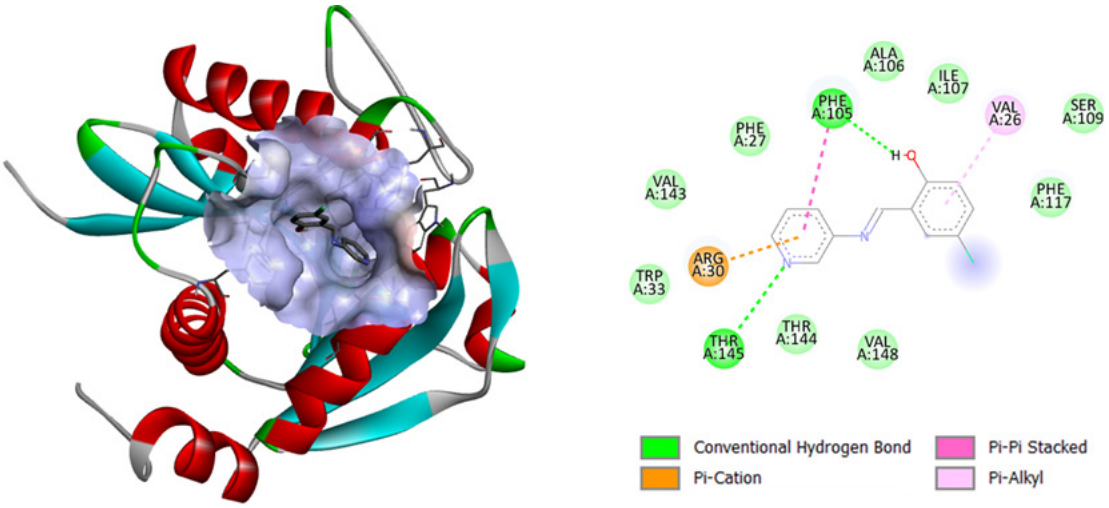


**Figure 12 –** Molecular docking results of compound **I** and *Pseudomonas aeruginosa* Synthase LasI

Generally, it is worth noting that the binding energies are close to each other, at a level of 5.5 – 6.5 kcal/mol. In most cases, the indicated energies are lower for the compound **I** than for the initial ligands (marked in bold in Table 7). At the same time, the affinity value comparable with that of used antibiotics is reached by the compound **I** only in the case of sortase B of *Staphylococcus aureus* and Lasl protein of *Pseudomonas aeruginosa*. For the last one the visualisation model of indicated interaction is presented in Figure 12. A binding of the molecule of enolimine form of compound **I** is is provided by hydrogen and π···π interactions with phenylalanine, π···alkyl interactions with valine, and hydrogen bonds with tyrosine. It is also worth noting the almost complete absence of differences in affinities between the tautomeric forms.

*Antimicrobial activity in vitro*

The method of obtaining the samples for *in vitro* testing is described in Section 2.9. An average mass of the compound **I** on the surface of each disc, determined according to the method described in Section 2.9, is about 10 μg, which roughly cor-

responds to the minimal inhibitory content of the substance isomeric to compound **I** that was determined in the paper [47]. At the same time the substance under study was present on the disc surface in its solid state. The results of the testing are collected in Table 8.

**Table 8 –** Bacteria growth inhibition zones around samples

| Bacteria | Growth inhibition zone (mm) | | |
|---|---|---|---|
| | Ti6Al4V | Ti6Al4V with calcium phosphate | Ti6Al4V with calcium phosphate and compound **I** |
| *Pseudomonas aeruginosa* | Continuous growth | 4±1 | 9±1 |
| *Escherichia coli* | Continuous growth | Continuous growth | Continuous growth |
| *Staphylococcus aureus* | Continuous growth | Continuous growth | Continuous growth |

As could be seen from the data of Table 8, no meaningful activity of the compound in relation to *Staphylococcus aureus* ATCC 25923, *Escherichia coli* ATCC 25922 was recorded, but a limited antimicrobial effect in relation to *Pseudomonas aeruginosa* ATCC 27853 was noted. For the alloy Ti6Al4V covered with calcium phosphate this effect might be related to the presence of $TiO_2$ on its surface.

*Toxicity of compound*

The toxicity of the compound **I** was estimated according to the ProTox online tool [84], and the predicted toxicity class is 4 out of 6, with $LD_{50}$ equal to 370 mg/kg. According to prediction, the compound might exhibit neurotoxicity, respiratory toxicity and immunotoxicity, and additionally be toxic to the environment. The detailed report is provided in Supplementary Information (Figure S1).

In order to check the effect of the compound on living organism, the *in vivo* tests with laboratory mice were conducted. Based on the visual inspection right after dissection, no abscesses or other local signs of inflammation were observed in any animal. The results of weighing the internal organs of the experimental animals are given in Table 9. To evaluated the organ conditions objectively, the ratios of the organ mass to the animal mass were calculated.

The results of determination of liver enzymes are summarised in Table 10.

**Table 9 –** Average masses of organs of laboratory mice at day 14 after injection of compound **I**

| Group | Weight of organs, g | | Weight of organs divided by weight of mouse | | Weight of mouse, g |
|---|---|---|---|---|---|
| | Heart | Liver | Heart | Liver | |
| Control | 0,108±0,004 | 1,26±0,07 | 0,0054±0,0003 | 0,063±0,005 | 20,0±0,5 |
| Injection of 0.2 mg/kg of compound **I** | 0,111±0,007 | 1,26±0,07 | 0,0045±0,0004 | 0,051±0,004 | 24,8±0,6 |

**Table 10 –** Activity of liver enzymes in the fresh blood samples of laboratory mice at day 14 after injection of compound **I**

| Group | Activity, U/l | |
|---|---|---|
| | Alanine aminotransferase | Aspartate transaminase |
| Norm [86] | 26 – 89 | 59 – 140 |
| Control | 74 ± 3 | 84 ± 7 |
| Injection of 0.2 mg/kg of compound **I** | 86 ± 2 | 86 ± 2 |

The results were compared using the Wilcoxon signed rank test [85], and neither organ masses, nor liver enzyme activities of mice in control and experimental groups revealed statistically significant differences. Although the darkening of the liver edges was noticed for the mice of experimental group, the activities of liver enzymes in the blood samples were still within their normal ranges [86]. The obtained data indicate that the implantation of compound **I** in the late postoperative period does not cause significant toxic shifts in the metabolism of mice.

*Intestinal absorption prediction pathway of compound*

The intestinal absorption pathway of the compound **I** was predicted using the SwissADME online tool [87], see Figure S2. According to the prediction, the compound has a good blood-brain barrier crossing probability. No active efflux of the compound by the P-glycoprotein is also predicted.

## Discussion

The combination of the presented results indicates the existence of the compound **I** predominantly in the enolimine form in the solid state. At the same time, in solutions in organic solvents, this form is also mainly present. With an increase in the polarity of the solvent, some displacement of the hydrogen atom from oxygen to the imine nitrogen takes place. Similar results are observed for a number of related compounds, including salicylideneaniline, salicylidene-2-aminopyridine, 5-chlorosalicylidene-2-aminopyridine [47, 80, 82]. In aqueous-alcoholic solutions of the compound **I**, the keto-enamine tautomeric form is present.

The obtained ionisation constant values correspond to dissociation of protonated pyridine nitrogen, protonation of imine nitrogen, and protonation of hydroxyl group

The molecular docking results indicate that only for some proteins the binding energies of the compound **I** are approaching those for ampicillin and azithromycin. For the related (and according to the data from [64] – the same) compound the values of minimum inhibitory concentration (MIC) in DMFA solution were evaluated in the paper [47], and these values are 30 times higher than these of ampicillin. This is fundamentally consistent with the calculated data presented in the present study. At the same time, fairly high level of toxicity of the compound **I** is assumed. Based on this it was quite important to test the antimicrobial activity of the compound under two given conditions. The first is the usage of a model that approximates the compound **I** to the real conditions of potential use on the implant surface. At the same time, the used form of the compound does not imply dissolution in toxic solvents. The second is testing the activity for low compound contents, in the MIC range for analogous substances. The results obtained indicate the prospects for using the compound **I** as an antimicrobial substance. Further work will be related to experimental studies related to the search for optimal antimicrobial activity with minimal toxicological impact on warm-blooded organisms.

## Conclusion

In the present study, the detailed results of computational studies of 4-chloro-2-((pyridin-3-ylimino) methyl)phenol is reported. The molecules in the crystal structure are mainly linked to each other by C–H···O and C–H···N hydrogen bonds. Most of the Hirschfeld surface is formed by mutual contacts of H···X (X = H, C, N, O, Cl) and C···X (X = C, N, O, Cl).

Comparison of the results of computer modeling and experimental studies indicates the predominant existence of the compound in the enolimine form in organic solvents. At the same time, the introduction of water leads to the appearance of the ketoenamine form.

The calculated results of molecular docking do not reveal any differences in the effect on a number of proteins of *Staphylococcus aureus* and *Pseudomonas aeruginosa*, while the affinity values themselves are either lower or are approaching those for reference antibiotics.

An inhibitory effect of microgram amounts of the compound on the surface of a medical titanium alloy on the development of *Pseudomonas aeruginosa* in vitro was detected.

No significant toxicity effects of the studied compound on the laboratory mice was detected.

## Supplementary Materials

The following supporting information is available: Figure S1 – The prediction of toxicity of the compound I by the Pro-Tox online tool; Figure S2 – The prediction of intestinal absorption and blood-brain barrier penetration of the compound I by the SwissADME online tool; Table S1 – Antibacterial activity of different secondary amines; Table S2 – Selected bond lengths (Å) and angles (°) in the optimized structure of cis-ketoenamine and trans-

ketoenamine form of compound I using the B3LYP/6-311++G(d,p) method; Table S3 – The vibration modes in the calculated IR spectrum (Figure 7) of the ground state of cis-ketoenamine form of compound I, obtained by using the DFT/B3LYP/6-311++G(d,p) method; Table S4 – The vibration modes in the calculated IR spectrum (Figure 7) of the ground state of trans-ketoenamine form of compound I, obtained by using the DFT/B3LYP/6-311++G(d,p) method.

**Acknowledgments**

This research was funded by Ministry of Science and Higher Education of Russian Federation, project topic "Materials and technologies for design and development of implants", state contract number 1023041400091-5-3.2.10;2.4.2.

The animal study protocol was approved by the Ethics Committee of Kurgan State University (protocol number 1 from 28th April 2025).

The authors are grateful to the pharmaceutical company Binnopharm Group for providing laboratory mice as the gift.

**Abbreviations**

The following abbreviations are used in this manuscript:

| | |
|---|---|
| HOMO | Highest occupied molecular orbital |
| LUMO | Lowest unoccupied molecular orbital |
| DFT | Density functional theory |
| NMR | Nuclear magnetic resonance |
| IR | Infrared |
| UV | Ultraviolet |
| MEP | Molecular electrostatic potential |
| MIC | Minimum inhibitory concentration |
| DMFA | Dimethylformamide |
| CCDC | The Cambridge Crystallographic Data Centre |
| LOD | Limit of detection |
| LOQ | Limit of quantification |
| NADH | Nicotinamide adenine dinucleotide |
| PDB | Protein databank |

**Conflict of interest**

The authors declare that they have no conflicts of interest.

**References**

1. Schiff, H. (1864). Eine neue Reihe organischer Basen. *Annalen der Chemie und Pharmacie*, vol. *131, no 1, pp.* 118–119.

2. Sacconi, L. (1966). Tetrahedral complexes of nickel(II) and copper(II) with schiff bases. *Coordination Chemistry Reviews, vol. 1, no 1–2*, pp. 126–132. https://doi.org/10.1016/s0010-8545(00)80165-4.

3. Li, P.; Niu, M.; Hong, M.; Cheng, S.; Dou, J. (2014). Effect of structure and composition of nickel(II) complexes with salicylidene Schiff base ligands on their DNA/protein interaction and cytotoxicity. *Journal of Inorganic Biochemistry, vol. 137*, pp. 101–108. https://doi.org/10.1016/j.jinorgbio.2014.04.005.

4. Aggarwal, N.; Kumar, R.; Dureja, P.; Rawat, D. S. (2009). Schiff bases as potential fungicides and nitrification inhibitors. *Journal of Agricultural and Food Chemistry*, vol. *57, no 18*, pp. 8520–8525. https://doi.org/10.1021/jf902035w.

5. Raczuk, E.; Dmochowska, B.; Samaszko-Fiertek, J.; Madaj, J. (2022). Different Schiff Bases–Structure, Importance and Classification. *Molecules*, vol. 27, no 3, article 787. https://doi.org/10.3390/molecules27030787.

6. Al-Amiery, A. A.; Al-Majedy, Y. K.; Ibrahim, H. H.; Al-Tamimi, A. A. (2012). Antioxidant, antimicrobial, and theoretical studies of the thiosemicarbazone derivative Schiff base 2-(2-imino-1-methylimidazolidin-4-ylidene)hydrazinecarbothioamide (IMHC). *Organic and Medicinal Chemistry Letters*, vol. *2, no 1, article* 4. https://doi.org/10.1186/2191-2858-2-4.

7. Ceyhan, G.; Çelik, C.; Uruş, S.; Demirtaş, İ.; Elmastaş, M.; Tümer, M. (2011). Antioxidant, electrochemical, thermal, antimicrobial and alkane oxidation properties of tridentate Schiff base ligands and their metal complexes. *Spectrochimica Acta Part A Molecular and Biomolecular Spectroscopy*, vol. *81, no 1*, pp. 184–198. https://doi.org/10.1016/j.saa.2011.05.106.

8. Mermer, A.; Demirbas, N.; Uslu, H.; Demirbas, A.; Ceylan, S.; Sirin, Y. (2019). Synthesis of novel Schiff bases using green chemistry techniques; antimicrobial, antioxidant, antiurease activity screening and molecular docking studies. *Journal of Molecular Structure*, vol. *1181*, pp. 412–422. https://doi.org/10.1016/j.molstruc.2018.12.114.

9. Teran, R.; Guevara, R.; Mora, J.; Dobronski, L.; Barreiro-Costa, O.; Beske, T.; Pérez-Barrera, J.; Araya-Maturana, R.; Rojas-Silva, P.; Poveda, A.; Heredia-Moya, J. (2019). Characterization of antimicrobial, antioxidant, and leishmanicidal activities of Schiff base derivatives of 4-Aminoantipyrine. *Molecules*, vol. *24, no 15*, article 2696. https://doi.org/10.3390/molecules24152696.

10. Hasi, Q.-M.; Fan, Y.; Yao, X.-Q.; Hu, D.-C.; Liu, J.-C. (2016). Synthesis, characterization, antioxidant and antimicrobial activities of a bidentate Schiff base ligand and its metal complexes. *Polyhedron*, vol. *109*, pp. 75–80. https://doi.org/10.1016/j.poly.2016.01.052.

11. Parekh, J.; Inamdhar, P.; Nair, R.; Baluja, S.; Chanda, S. (2005). Synthesis and antibacterial activity of some Schiff bases derived from 4-aminobenzoic acid. *Journal of the Serbian Chemical Society*, vol. *70, no 10*, pp. 1155–1162. https://doi.org/10.2298/jsc0510155p.

12. Imran, S.; Taha, M.; Ismail, N.; Khan, K.; Naz, F.; Hussain, M.; Tauseef, S. (2014). Synthesis of Novel Bisindolylmethane Schiff bases and Their Antibacterial Activity. *Molecules*, vol. *19, no 8*, pp. 11722–11740. https://doi.org/10.3390/molecules190811722.

13. Nair, R.; Shah, A.; Baluja, S.; Chanda, S. (2006). Synthesis and antibacterial activity of some Schiff base complexes. *Journal of the Serbian Chemical Society, vol. 71, no 7*, pp. 733–744. https://doi.org/10.2298/jsc0607733n.

14. Tehrani, K. H. M. E.; Hashemi, M.; Hassan, M.; Kobarfard, F.; Mohebbi, S. (2015). Synthesis and antibacterial activity of Schiff bases of 5-substituted isatins. *Chinese Chemical Letters*, vol. *27, no 2*, pp. 221–225. https://doi.org/10.1016/j.cclet.2015.10.027.

15. Malladi, S.; Isloor, A. M.; Isloor, S.; Akhila, D. S.; Fun, H.-K. (2011). Synthesis, characterization and antibacterial activity of some new pyrazole based Schiff bases. *Arabian Journal of Chemistry*, vol. *6, no 3, pp.* 335–340. https://doi.org/10.1016/j.arabjc.2011.10.009.

16. Chohan, Z. H.; Scozzafava, A.; Supuran, C. T. (2003). Zinc Complexes of Benzothiazole-derived Schiff Bases with Antibacterial Activity. *Journal of Enzyme Inhibition and Medicinal Chemistry*, vol. *18, no 3, pp.* 259–263. https://doi.org/10.1080/14756360310000071817.

17. Vashi, K.; Naik, H. B. (2004). Synthesis of Novel Schiff Base and Azetidinone Derivatives and their Antibacterial Activity. *Journal of Chemistry*, vol. *1, no 5, pp.* 272–275. https://doi.org/10.1155/2004/158924.

18. Asiri, A. M.; Khan, S. A. (2010). Synthesis and Anti-Bacterial Activities of Some Novel Schiff Bases Derived from Aminophenazone. *Molecules*, vol. *15, no 10, pp.* 6850–6858. https://doi.org/10.3390/molecules15106850.

19. Mondal, S.; Mandal, S. M.; Mondal, T. K.; Sinha, C. (2015). Structural characterization of new Schiff bases of sulfamethoxazole and sulfathiazole, their antibacterial activity and docking computation with DHPS protein structure. *Spectrochimica Acta Part A Molecular and Biomolecular Spectroscopy*, vol. *150*, pp. 268–279. https://doi.org/10.1016/j.saa.2015.05.049.

20. Cheng, K.; Zheng, Q.-Z.; Qian, Y.; Shi, L.; Zhao, J.; Zhu, H.-L. (2009). Synthesis, antibacterial activities and molecular docking studies of peptide and Schiff bases as targeted antibiotics. *Bioorganic & Medicinal Chemistry*, vol. *17, no 23, pp.* 7861–7871. https://doi.org/10.1016/j.bmc.2009.10.037.

21. El-Gammal, O. A.; Mohamed, F. Sh.; Rezk, G. N.; El-Bindary, A. A. (2021). Synthesis, characterization, catalytic, DNA binding and antibacterial activities of Co(II), Ni(II) and Cu(II) complexes with new Schiff base ligand. *Journal of Molecular Liquids*, vol. *326*, article 115223. https://doi.org/10.1016/j.molliq.2020.115223.

22. Wang, X.; Yin, J.; Shi, L.; Zhang, G.; Song, B. (2014). Design, synthesis, and antibacterial activity of novel Schiff base derivatives of quinazolin-4(3H)-one. *European Journal of Medicinal Chemistry*, vol. *77*, pp. 65–74. https://doi.org/10.1016/j.ejmech.2014.02.053.

23. Anacona, J. R.; Rodriguez, J. L.; Camus, J. (2014). Synthesis, characterization and antibacterial activity of a Schiff base derived from cephalexin and sulphathiazole and its transition metal complexes. *Spectrochimica Acta Part A Molecular and Biomolecular Spectroscopy*, vol. *129*, pp. 96–102. https://doi.org/10.1016/j.saa.2014.03.019.

24. Goszczyńska, A.; Kwiecień, H.; Fijałkowski, K. (2015). Synthesis and antibacterial activity of Schiff bases and amines derived from alkyl 2-(2-formyl-4-nitrophenoxy)alkanoates. *Medicinal Chemistry Research*, vol. *24, no 9, pp.* 3561–3577. https://doi.org/10.1007/s00044-015-1397-6.

25. Ommenya, F. K.; Nyawade, E. A.; Andala, D. M.; Kinyua, J. (2020). Synthesis, Characterization and Antibacterial Activity of Schiff Base, 4-Chloro-2-{(E)-[(4-Fluorophenyl)imino]methyl}phenol Metal (II) Complexes. *Journal of Chemistry*, vol. *2020*, article 1745236. https://doi.org/10.1155/2020/1745236.

26. Reiss, A.; Florea, S.; Caproiu, T.; Stanica, N. (2009). Synthesis, characterization, and antibacterial activity of some transition metals with the Schiff base N-(2-furanylmethylene)-3-aminodibenzofuran. *Turkish Journal of Chemistry*, vol. *33, no 6, pp.* 775–783. https://doi.org/10.3906/kim-0807-31.

27. Chaudhary, N. K.; Mishra, P. (2017). Metal complexes of a novel Schiff base based on penicillin: characterization, molecular modeling, and antibacterial activity study. *Bioinorganic Chemistry and Applications*, vol. *2017*, article 6927675. https://doi.org/10.1155/2017/6927675.

28. Yin, X.; Chen, J.; Yuan, W.; Lin, Q.; Ji, L.; Liu, F. (2011). Preparation and antibacterial activity of Schiff bases from O-carboxymethyl chitosan and para-substituted benzaldehydes. *Polymer Bulletin*, vol. *68, no 5, pp.* 1215–1226. https://doi.org/10.1007/s00289-011-0599-4.

29. Hadjoudis, E.; Vittorakis, M.; Moustakali-Mavridis, I. (1987). Photochromism and thermochromism of schiff bases in the solid state and in rigid glasses. *Tetrahedron*, vol. *43, no 7, pp.* 1345–1360. https://doi.org/10.1016/s0040-4020(01)90255-8.

30. Ogawa, K.; Kasahara, Y.; Ohtani, Y.; Harada, J. (1998). Crystal structure change for the thermochromy of N-Salicylideneanilines. the first observation by x-ray diffraction. *Journal of the American Chemical Society*, vol. *120, no 28, pp.* 7107–7108. https://doi.org/10.1021/ja980972v.

31. Alarcón, S. H.; Olivieri, A. C.; Sanz, D.; Claramunt, R. M.; Elguero, J. (2004). Substituent and solvent effects on the proton transfer equilibrium in anils and azo derivatives of naphthol. Multinuclear NMR study and theoretical calculations. *Journal of Molecular Structure*, vol. *705, no 1–3*, pp. 1–9. https://doi.org/10.1016/s0022-2860(03)00208-4.

32. Filarowski, A.; Koll, A.; Sobczyk, L. (2009). Intramolecular Hydrogen Bonding in o-hydroxy Aryl Schiff Bases. *Current Organic Chemistry*, vol. *13, no 2, pp.* 172–193. https://doi.org/10.2174/138527209787193765.

33. Minkin, V. I.; Tsukanov, A. V.; Dubonosov, A. D.; Bren, V. A. (2011). Tautomeric Schiff bases: Iono-, solvato-, thermo- and photochromism. *Journal of Molecular Structure*, vol. *998, no* 1–3, pp. 179–191. https://doi.org/10.1016/j.molstruc.2011.05.029.

34. Zhao, J.; Ji, S.; Chen, Y.; Guo, H.; Yang, P. (2011). Excited state intramolecular proton transfer (ESIPT): from principal photophysics to the development of new chromophores and applications in fluorescent molecular probes and luminescent materials. *Physical Chemistry Chemical Physics*, vol. *14, no 25, pp.* 8803–8817. https://doi.org/10.1039/c2cp23144a.

35. Hadjoudis, E.; Chatziefthimiou, S.; Mavridis, I. (2009). Anils: Photochromism by H-Transfer. *Current Organic Chemistry*, vol. *13, no 3, pp.* 269–286. https://doi.org/10.2174/138527209787314797.

36. Panchal, P. K.; Parekh, H. M.; Pansuriya, P. B.; Patel, M. N. (2006). Bactericidal activity of different oxovanadium(IV) complexes with Schiff bases and application of chelation theory. *Journal of Enzyme Inhibition and Medicinal Chemistry*, vol. *21, no 2, pp.* 203–209. https://doi.org/10.1080/14756360500535229.

37. Yildirim, N.; Yildiz, M. (2018). A Schiff base sensor selective to anions, biological activity and spectral studies. *Journal of the Turkish Chemical Society Section A Chemistry*, vol. *5, no 3*, pp. 1271–1278. https://doi.org/10.18596/jotcsa.431554.

38. Yıldız, M.; Karpuz, Ö.; Zeyrek, C. T.; Boyacıoğlu, B.; Dal, H.; Demir, N.; Yıldırım, N.; Ünver, H. (2015). Synthesis, biological activity, DNA binding and anion sensors, molecular structure and quantum chemical studies of a novel bidentate Schiff base derived from 3,5-bis(triflouromethyl)aniline and salicylaldehyde. *Journal of Molecular Structure*, vol. *1094*, pp. 148–160. https://doi.org/10.1016/j.molstruc.2015.03.047.

39. Dege, N.; Gökce, H.; Doğan, O. E.; Alpaslan, G.; Ağar, T.; Muthu, S.; Sert, Y. (2022). Quantum computational, spectroscopic investigations on N-(2-((2-chloro-4,5-dicyanophenyl)amino)ethyl)-4-methylbenzenesulfonamide by DFT/TD-DFT with different solvents, molecular docking and drug-likeness researches. *Colloids and Surfaces A Physicochemical and Engineering Aspects*, vol. *638*, article 128311. https://doi.org/10.1016/j.colsurfa.2022.128311.

40. Yıldız, M.; Tan, E.; Demir, N.; Yıldırım, N.; Ünver, H.; Kiraz, A.; Mestav, B. (2015). Synthesis and spectral, antimicrobial, anion sensing, and DNA binding properties of Schiff base podands and their metal complexes. *Russian Journal of General Chemistry*, vol. *85, no 9, pp.* 2149–2162. https://doi.org/10.1134/s1070363215090200.

41. Adeel-Sharif, H. M.; Ahmed, D.; Mir, H. (2015). Antimicrobial salicylaldehyde Schiff bases: synthesis, characterization and evaluation. *Pakistan Journal of Pharmaceutical Sciences*, vol. *28, no 2, pp.* 449–455.

42. Shi, L.; Ge, H.-M.; Tan, S.-H.; Li, H.-Q.; Song, Y.-C.; Zhu, H.-L.; Tan, R.-X. (2006). Synthesis and antimicrobial activities of Schiff bases derived from 5-chloro-salicylaldehyde. *European Journal of Medicinal Chemistry*, vol. *42, no 4, pp.* 558–564. https://doi.org/10.1016/j.ejmech.2006.11.010.

43. Montaser, A. S.; Wassel, Ahmed. R.; Al-Shaye'a, O. N. (2018). Synthesis, characterization and antimicrobial activity of Schiff bases from chitosan and salicylaldehyde/$TiO_2$ nanocomposite membrane. *International Journal of Biological Macromolecules*, vol. *124*, pp. 802–809. https://doi.org/10.1016/j.ijbiomac.2018.11.229.

44. Jesmin, M.; Ali, M. M.; Salahuddin, M. S.; Habib, M. R.; Khanam, J. A. (2008). Antimicrobial Activity of Some Schiff Bases Derived from Benzoin, Salicylaldehyde, Aminophenol and 2,4 Dinitrophenyl Hydrazine. *Mycobiology*, vol. *36, no 1, article* 70. https://doi.org/10.4489/myco.2008.36.1.070.

45. Jampilek, J. (2019). Heterocycles in medicinal chemistry. *Molecules*, vol. *24, no 21, article* 3839. https://doi.org/10.3390/molecules24213839.

46. Heravi, M. M.; Zadsirjan, V. (2020). Prescribed drugs containing nitrogen heterocycles: an overview. *RSC Advances*, vol. *10, no 72, pp.* 44247–44311. https://doi.org/10.1039/d0ra09198g.

47. Yildirim, N.; Demir, N.; Alpaslan, G.; Boyacioğlu, B.; Yildiz, M.; Ünver, H. (2018). DFT calculation, biological activity, anion sensing studies and crystal structure of (E)-4-chloro-2-((pyridin-2-ylimino)-methyl)phenol. *Journal of the Serbian Chemical Society*, vol. *83, no 6, pp.* 707–721. https://doi.org/10.2298/jsc171001009y.

48. Dueke-Eze; Fasina, C. U.; Idika. (2011). Synthesis, electronic spectra and inhibitory study of some Salicylaldehyde Schiff bases of 2-aminopyridine. *African Journal of Pure and Applied Chemistry*, vol. *5, no 2, pp.* 13–18. https://doi.org/10.5897/ajpac.9000160.

49. Barboza, C. A.; Germino, J. C.; Duarte, L. G. T. A.; Quites, F. J.; Vazquez, P. A. M.; Atvars, T. D. Z. (2016). Photoacidity of the N -salicylidene-5-chloroaminopyridine. *Journal of Luminescence*, vol. *184*, pp. 268–272. https://doi.org/10.1016/j.jlumin.2016.12.045.

50. Sliwa, M.; Mouton, N.; Ruckebusch, C.; Aloïse, S.; Poizat, O.; Buntinx, G.; Métivier, R.; Nakatani, K.; Masuhara, H.; Asahi, T. (2009). Comparative investigation of ultrafast photoinduced processes in Salicylidene-Aminopyridine in solution and solid state. *The Journal of Physical Chemistry C*, vol. *113, no 27, pp.* 11959–11968. https://doi.org/10.1021/jp901849a.

51. Zhao, L.; Sui, D.; Wang, Y. (2015). Luminescent properties of N-salicylidene-3-aminopyridine and selective sensing behavior to $Ba^{2+}$. *Journal of Luminescence*, vol. *162*, pp. 81–86. https://doi.org/10.1016/j.jlumin.2015.02.038.

52. Moustakali-Mavridis, I.; Hadjoudis, E.; Mavridis, A. (1978). Crystal and molecular structure of some thermochromic Schiff bases. *Acta Crystallographica Section B*, vol. *34, no 12, pp.* 3709–3715. https://doi.org/10.1107/s0567740878011930.

53. Goyat, G.; Malik, A.; Vikas; Verma, K. K.; Garg, S. (2018). Spectroscopic and Biological Studies of 3,5-Dichlorosalicylaldehyde-3-Aminopyridine Schiff Base and their Tellurium(IV) Complexes. *International Journal of Scientific Research in Science Engineering and Technology*, vol. *4, no 1, pp.* 755–762. https://doi.org/10.32628/ijsrset1841205.

54. Moustakali-Mavridis, I.; Hadjoudis, B.; Mavridis, A. (1980). Structure of thermochromic Schiff bases. II. Structures of N-salicylidene-3-aminopyridine and N-(5-methoxysalicylidene)-3-aminopyridine. *Acta Crystallographica Section B*, vol. *36, no 5, pp.* 1126–1130. https://doi.org/10.1107/s0567740880005432.

55. Vinita, G.; Sanchita, S.; Gupta, Y. K. (2013). Synthesis and Antimicrobial Activity of some Salicylaldehyde Schiff bases of 2-aminopyridine. *Research Journal of Chemical Sciences*, vol. *3, no 9, pp.* 26–29.

56. Cimerman, Z.; Galic, N.; Bosner, B. (1997). The Schiff bases of salicylaldehyde and aminopyridines as highly sensitive analytical reagents. *Analytica Chimica Acta*, vol. *343, no 1–2*, pp. 145–153. https://doi.org/10.1016/s0003-2670(96)00587-9.

57. Angyl, S. J.; Angyal, C. L. (1952). 268. The tautomerism of N-hetero-aromatic amines. Part I. *Journal of the Chemical Society (Resumed)*, pp. 1461–1466. https://doi.org/10.1039/jr9520001461.

58. Bates, R. G. (1964). *Determination of pH, Theory and Practice.* Wiley, New York, pp. 222-230.

59. Gelsema, W. J.; De Ligny, C. L.; Remijnse, A. G.; Blijleven, H. A. (1966). pH-Measurements in alcohol-water mixtures, using aqueous standard buffer solutions for calibration. *Recueil Des Travaux Chimiques Des Pays-Bas*, vol. *85, no 7, pp.* 647–660. https://doi.org/10.1002/recl.19660850702.

60. Spackman, M. A.; Jayatilaka, D. (2008). Hirshfeld surface analysis. *CrystEngComm*, vol. *11, no 1, pp.* 19–32. https://doi.org/10.1039/b818330a.

61. Spackman, M. A.; McKinnon, J. J. (2002). Fingerprinting intermolecular interactions in molecular crystals. *CrystEngComm*, vol. *4, no 66, pp.* 378–392. https://doi.org/10.1039/b203191b.

62. Spackman, P. R.; Turner, M. J.; McKinnon, J. J.; Wolff, S. K.; Grimwood, D. J.; Jayatilaka, D.; Spackman, M. A. (2021). CrystalExplorer: a program for Hirshfeld surface analysis, visualization and quantitative analysis of molecular crystals. *Journal of Applied Crystallography*, vol. *54, no 3, pp.* 1006–1011. https://doi.org/10.1107/s1600576721002910.

63. Rodić, M. (2020). CCDC 1869718: Experimental Crystal Structure Determination. *The Cambridge Structural Database*. https://doi.org/10.5517/ccdc.csd.cc20rlhw.

64. Rodić, M. (2018). Comments on DFT calculation, biological activity, anion sensing studies and crystal structure of (E)-4-chloro-2-((pyridin-2-ylimino)-methyl)phenol by Nuray Yıldırım, Neslihan Demir, Gökhan Alpaslan, Bahadir Boyacıoğlu, Mustafa Yıldız, and Huseyin Ünver, published in the Journal of the Serbian Chemical Society, volume 83, issue 6, 2018, pp. 707-721. *Journal of the Serbian Chemical Society*, vol. *84, no 1, pp.* 111–116. https://doi.org/10.2298/jsc180925082r.

65. Dennington, R.; Keith, T. A.; Millam, J. M. (2016). *GaussView Version 6.0.* Semichem Inc., Shawnee Mission, KS.

66. Frisch, M.J.; Trucks, G.W.; Schlegel, H.B.; Scuseria, G.E.; Robb, M.A.; Cheeseman, J.R.; Scalmani, G.; Barone, V.; Mennucci, B.; Petersson, G.A. et al. (2009). *Gaussian 09, Revision D.01*. Gaussian. Inc., Wallingford.

67. Krishnan, R.; Binkley, J. S.; Seeger, R.; Pople, J. A. (1980). Self-consistent molecular orbital methods. XX. A basis set for correlated wave functions. *The Journal of Chemical Physics*, vol. *72, no 1, pp.* 650–654. https://doi.org/10.1063/1.438955.

68. Becke, A. D. (1993). Density-functional thermochemistry. III. The role of exact exchange. *The Journal of Chemical Physics*, vol. *98, no 7, pp.* 5648–5652. https://doi.org/10.1063/1.464913.

69. Frisch, M. J.; Pople, J. A.; Binkley, J. S. (1984). Self-consistent molecular orbital methods 25. Supplementary functions for Gaussian basis sets. *The Journal of Chemical Physics*, vol. *80, no 7, pp.* 3265–3269. https://doi.org/10.1063/1.447079.

70. Jamróz, M. H. (2013). Vibrational Energy Distribution Analysis (VEDA): Scopes and limitations. *Spectrochimica Acta Part A Molecular and Biomolecular Spectroscopy*, vol. *114*, pp. 220–230. https://doi.org/10.1016/j.saa.2013.05.096.

71. Berman, H. M.; Battistuz, T.; Bhat, T. N.; Bluhm, W. F.; Bourne, P. E.; Burkhardt, K.; Feng, Z.; Gilliland, G. L.; Iype, L.; Jain, S.; Fagan, P.; Marvin, J.; Padilla, D.; Ravichandran, V.; Schneider, B.; Thanki, N.; Weissig, H.; Westbrook, J. D.; Zardecki, C. (2002). The Protein Data Bank. *Acta Crystallographica Section D Biological Crystallography*, vol. *58, no 6, pp.* 899–907. https://doi.org/10.1107/s0907444902003451.

72. Trott, O.; Olson, A. J. (2009). AutoDock Vina: Improving the speed and accuracy of docking with a new scoring function, efficient optimization, and multithreading. *Journal of Computational Chemistry*, vol. *31, no 2, pp.* 455–461. https://doi.org/10.1002/jcc.21334.

73. Morris, G. M.; Huey, R.; Lindstrom, W.; Sanner, M. F.; Belew, R. K.; Goodsell, D. S.; Olson, A. J. (2009). AutoDock4 and AutoDockTools4: Automated docking with selective receptor flexibility. *Journal of Computational Chemistry*, vol. *30, no 16, pp.* 2785–2791. https://doi.org/10.1002/jcc.21256.

74. Kuo, M. C.; Yen, S. K. (2002). The process of electrochemical deposited hydroxyapatite coatings on biomedical titanium at room temperature. *Materials Science and Engineering C*, vol. *20, no 1–2*, pp. 153–160. https://doi.org/10.1016/s0928-4931(02)00026-7.

75. Zhang, Y.-Y.; Tao, J.; Pang, Y.-C.; Wang, W.; Wang, T. (2006). Electrochemical deposition of hydroxyapatite coatings on titanium. *Transactions of Nonferrous Metals Society of China*, vol. *16, no 3, pp.* 633–637. https://doi.org/10.1016/s1003-6326(06)60112-x.

76. McFarland, J. (1907). The nephelometer: an instrument for media used for estimating the number of bacteria in suspensions used for calculating the opsonic index and for vaccines. *Journal of American Medical Association*, vol. 49, no 14, pp. 1176-1178. 10.1001/jama.1907.25320140022001f.

77. Arnold, P. M.; Parslow, G. R. (1995). Designing a coupled assay system for aspartate aminotransferase. *Biochemical Education*, vol. *23, no 1, pp.* 40–41. https://doi.org/10.1016/0307-4412(94)00116-7.

78. Banfi, D.; Patiny, L. (2008). www.nmrdb.org: Resurrecting and processing NMR spectra on-line *Chimia*, vol. *62, no 4, pp.* 280-281. https://doi.org/10.2533/chimia.2008.280.

79. Jelsch, C.; Ejsmont, K.; Huder, L. (2014). The enrichment ratio of atomic contacts in crystals, an indicator derived from the Hirshfeld surface analysis. *International Union of Crystallography Journal*, vol. *1, no 2, pp.* 119–128. https://doi.org/10.1107/s2052252514003327.

80. Moosavi-Tekyeh, Z.; Dastani, N. (2015). Intramolecular hydrogen bonding in N-salicylideneaniline: FT-IR spectrum and quantum chemical calculations. *Journal of Molecular Structure*, vol. *1102*, pp. 314–322. https://doi.org/10.1016/j.molstruc.2015.09.001.

81. Geerlings, P.; De Proft, F.; Langenaeker, W. (2003). Conceptual Density Functional Theory. *Chemical Reviews*, vol. *103, no 5, pp.* 1793–1874. https://doi.org/10.1021/cr990029p.

82. Galić, N.; Cimerman, Z.; Tomišić, V. (1997). Tautomeric and protonation equilibria of Schiff bases of salicylaldehyde with aminopyridines. *Analytica Chimica Acta*, vol. *343, no 1–2*, pp. 135–143. https://doi.org/10.1016/s0003-2670(96)00586-7.

83. Meshkov, A. N.; Gamov, G. A. (2019). KEV: A free software for calculating the equilibrium composition and determining the equilibrium constants using UV–Vis and potentiometric data. *Talanta*, vol. *198*, pp. 200–205. https://doi.org/10.1016/j.talanta.2019.01.107.

84. Banerjee, P.; Kemmler, E.; Dunkel, M.; Preissner, R. (2024). ProTox 3.0: a webserver for the prediction of toxicity of chemicals. *Nucleic Acids Research*, vol. *52, no W1, pp.* W513–W520. https://doi.org/10.1093/nar/gkae303.

85. Wilcoxon, F. (1945). Individual comparisons by ranking methods. *Biometrics Bulletin*, vol. *1, no 6, pp.* 80–83. https://doi.org/10.2307/3001968.

86. Mirošnikov, M. V.; Makarova, M. N. (2021). Variabel'nost' biohimičeskih pokazatelej krovi i ustanovlenie referensnyh intervalov v dokliničeskih issledovaniâh. Soobŝenie 4: myši. *Laboratornye životnye dlâ naučnyh issledovanij*, no *3*, pp. 63–69. https://doi.org/10.29296/2618723X-2021-03-08.

87. Daina, A.; Zoete, V. (2016). A BOILED-Egg to predict gastrointestinal absorption and brain penetration of small molecules. *ChemMedChem*, vol. *11, no 11, pp.* 1117–1121. https://doi.org/10.1002/cmdc.201600182.

***Information about authors:***

*Artem V. Sharov – PhD, Senior Researcher, Laboratory of Advanced Materials for Industry and Biomedicine, Kurgan State University (Kurgan, Russia, e-mail: sharow84@gmail.com)*

*Pavel A. Nikolaychuk – PhD, Senior Researcher, Scientific-Educational Centre of Chemistry and Chemical Technology of Novosibirsk State University (Novosibirsk, Russia, e-mail: pavel.nikolaychuk@kgsu.ru)*

*Anastasia A. Tereshkina –M. Sc. Junior Researcher, Ural Federal University named after the first President of Russia Boris Nikolaevich Yeltsin (Yekaterinburg, Russia, e-mail: an-terrr@mail.ru)*

*Alena V. Dostovalova – M.Sc., Junior Researcher, Laboratory of Advanced Materials for Industry and Biomedicine, Kurgan State University (Kurgan, Russia, e-mail: alenka_01_45@mail.ru)*

*Yulia A. Enova – M.Sc., Junior Researcher, Laboratory of Advanced Materials for Industry and Biomedicine, Kurgan State University (Kurgan, Russia, e-mail: julia_qwer19@mail.ru)*

*Darya S. Popova – M.Sc., Junior Researcher, Laboratory of Advanced Materials for Industry and Biomedicine, Kurgan State University (Kurgan, Russia, e-mail: nikitina.dar@mail.ru)*

*Darya A. Rychkova – M.Sc., Junior Researcher, Laboratory of Advanced Materials for Industry and Biomedicine, Kurgan State University (Kurgan, Russia, e-mail: dariaruchkova25@gmail.com)*

*Alena Y. Kurochkina – M.Sc., Junior Researcher, Laboratory of Advanced Materials for Industry and Biomedicine, Kurgan State University (Kurgan, Russia, e-mail: aleona.kurochkina@yandex.ru)*

*Valentina V. Savinova – M.Sc., Junior Researcher, Laboratory of Advanced Materials for Industry and Biomedicine, Kurgan State University (Kurgan, Russia, e-mail: savinovavalenrina21@mail.ru)*

*Aleksander N. Nakoskin – PhD, Senior Researcher, Laboratory of Advanced Materials for Industry and Biomedicine, Kurgan State University (Kurgan, Russia, e-mail: Nakoskin_A@mail.ru)*

*Irina V. Shipitsyna – PhD, Researcher, National Ilizarov Medical Research Centre for Traumatology and Orthopaedics (Kurgan, Russia, e-mail: IVSchimik@mail.ru)*

*Oleg V. Filisteev – PhD, Senior Researcher, Laboratory of Advanced Materials for Industry and Biomedicine, Kurgan State University (Kurgan, Russia, e-mail: filisteev.oleg@gmail.com)*

*Soe T. Lwin – PhD, Senior Researcher, Medical Research Centre (Nay Pyi Taw, Myanmar, e-mail: drthihalwin2012@gmail.com)*

*Min M. Zaw – PhD, Senior Researcher, Medical Research Centre (Nay Pyi Taw, Myanmar, e-mail: mrzaw710@gmail.com)*

*Zaw Minthein – PhD, Senior Researcher, Medical Academy (Yangon, Myanmar, e-mail: zawminthein@gmail.com)*

*Zaw Y.M. Oo – PhD, Senior Researcher, Science Research Centre of the Republic of the Union of Myanmar (Nay Pyi Taw, Myanmar, e-mail: zawyemawoo@gmail.com)*